

# NUMERICAL MODELING OF POSITRON ANNHILITATION

by

Josh Heiner

A senior thesis submitted to the faculty of

Brigham Young University - Idaho

in partial fulfillment of the requirements for the degree of

Bachelor of Science

Department of Physics

Brigham Young University - Idaho

April 2014



Copyright © 2014 Josh Heiner

All Rights Reserved



BRIGHAM YOUNG UNIVERSITY - IDAHO

DEPARTMENT APPROVAL

of a senior thesis submitted by

Josh Heiner

This thesis has been reviewed by the research committee, senior thesis coordinator, and department chair and has been found to be satisfactory.

---

Date

Evan Hansen, Advisor

---

Date

David Oliphant, Senior Thesis Coordinator

---

Date

Richard Hatt, Committee Member

---

Date

Stephen McNeil, Department Chair



## ABSTRACT

### NUMERICAL MODELING OF POSITRON ANNHILITATION

Josh Heiner

Department of Physics

Bachelor of Science

Computational positron spectroscopy involves modeling elements or compounds accurately and comparing those models with experimental data. This is done by becoming proficient at space groups and solid state physics, analyzing data, and convoluting data outputs. My research uses the MIKA/Doppler program, which calculates the Density Functional Theory (DFT) to help model and understand what is happening in a given unit cell. I will give a brief background information on density functional theory, multigrid methods, and the challenges that are faced before using the MIKA program. These include converting between coordinate systems, understanding space groups, and symmetries in solid state physics. An understanding of convolution theory is needed to manipulate the MIKA output before it is ready to be analyzed. This modeling helps in understanding defects, impurities, and solubilities in elements and compounds. Copper, ice 1<sub>h</sub>, and silicon dioxide will be represented and

analyzed in this thesis.

## ACKNOWLEDGMENTS

My life changed when I met and married my wife Debra. She puts up with a lot and I would not be the same without her and Billy. Her willingness to allow me to continue working all day without much interaction is very much appreciated and often overlooked on my part. Debra, I love you.

I would like to express my thanks to my mother Diana. Even when I am in the wrong she will defend at all costs. My father Dick expects the very best from me and that is why I work as much as I do. Both show their love and appreciation for me which helps build me.

I am particularly grateful for the physics faculty at BYU-Idaho. As a group the department carries a lot of knowledge and are always willing to share and lift students. The faculty has such a diverse and good methods of teaching; it was fun learning and growing.



# Contents

<b>Table of Contents</b>	<b>xi</b>
<b>List of Figures</b>	<b>xiii</b>
<b>1 Introduction</b>	<b>1</b>
1.1 Overview . . . . .	1
1.2 Use of PAS . . . . .	2
1.3 Annihilation Background . . . . .	3
1.4 Crystallography Background . . . . .	6
<b>2 Method</b>	<b>11</b>
2.1 The Wave Equation . . . . .	11
2.2 Density Functional Theory . . . . .	12
2.3 Multigrid Methods . . . . .	16
2.4 Annihilation . . . . .	20
2.5 Simulation . . . . .	21
<b>3 Procedure</b>	<b>25</b>
3.1 Crystalline Structure . . . . .	25
3.2 INPUT . . . . .	26
3.3 Manipulation . . . . .	28
<b>4 Copper</b>	<b>33</b>
4.1 Copper Pure . . . . .	33
4.2 Copper Vacancy . . . . .	36
4.3 Copper Defects . . . . .	37
4.4 Copper Analysis . . . . .	38
<b>5 Ice 1<sub>h</sub></b>	<b>41</b>
5.1 Ice Pure . . . . .	41
5.2 Ice Vacancy . . . . .	42
5.3 Ice Analysis . . . . .	44

---

<b>6 Silicon Dioxide</b>	<b>47</b>
6.1 SiO <sub>2</sub> Pure and Vacancy . . . . .	47
6.2 SiO <sub>2</sub> Analysis . . . . .	49
<b>7 Conclusion</b>	<b>53</b>
7.1 Analysis . . . . .	53
7.2 Error . . . . .	54
7.3 Future Research . . . . .	55
<b>Bibliography</b>	<b>57</b>
<b>A Crystallography</b>	<b>59</b>
<b>B INPUT H<sub>2</sub>O _ 36</b>	<b>63</b>
<b>Index</b>	<b>67</b>

# List of Figures

1.1	Tools for microstructure probing . . . . .	3
1.2	Annihilation of positron and electron . . . . .	4
1.3	Positron-Electron Wave Interactions . . . . .	6
1.4	Phase diagram of water . . . . .	8
2.1	Electron density of Copper . . . . .	13
2.2	Pseudopotential . . . . .	15
2.3	Positron density of Copper . . . . .	17
2.4	Multigrid Error . . . . .	18
2.5	Multigrid levels vs time . . . . .	19
2.6	Wave Interaction Simulation . . . . .	22
2.7	Annihilation Rate and Lifetime Simulation . . . . .	23
3.1	Coordinate Transfer . . . . .	26
3.2	Crystalline Structure of Silicon Dioxide . . . . .	28
3.3	Momentum distribution of Copper . . . . .	30
3.4	Decomposed momentum distributions of Copper . . . . .	31
4.1	Copper with Positron and Electron densities . . . . .	34
4.2	Copper momentum with computation and experimental . . . . .	35
4.3	Copper Positron Density with vacancy . . . . .	36
4.4	Copper Electron Density with Hydrogen . . . . .	37
4.5	Copper Positron Density with Hydrogen . . . . .	38
4.6	Copper vacancy, defect, and pure momentum distributions . . . . .	39
4.7	Parameter compared for copper . . . . .	40
5.1	Electron Density in Ice . . . . .	42
5.2	Crystalline structure of ice 1 <sub>h</sub> . . . . .	43
5.3	Momentum Distribution pure ice . . . . .	44
5.4	Momentum Distribution pure and vacancy ice . . . . .	45
5.5	Parameter compared for ice . . . . .	46
6.1	Electron density of Silicon Dioxide . . . . .	48
6.2	Decomposed momentum distribution Silicon Dioxide . . . . .	49

6.3	Momentum distribution Silicon Dioxide with vacancy . . . . .	50
6.4	Parameter compared for silicon dioxide . . . . .	50
6.5	Sio <sub>2</sub> Decomposed Momentum Distribution in Pure and Si poor . . .	51

# Chapter 1

## Introduction

### 1.1 Overview

Positron annihilation spectroscopy (PAS) is well recognized as a powerful tool of microstructure investigations of condensed matter [1]. This is an effective non-destructive method to probe a microstructure. As raw data is collected, scientists urge for a method to describe and predict what is happening. The need becomes constant for an accurate numerical method to describe what is occurring.

The computational analysis of positron annihilation spectroscopy predicts what should be observed experimentally. As defects and impurities are introduced into the structure, it will show with changes in the output. This information is used in the comparison of the experimental data that has impurities and defects.

For the computational analysis, the program MIKA (Multi-grid Instead of K-spAce) Doppler was used. This program was written at the Helsinki University of Technology and has been an accepted computational program [2]. MIKA is freely available for anyone and is mostly used by researchers in the electronic structure community.

To use MIKA, a strong knowledge was needed in understanding and building crystalline structure. The source of most of the information was "Space groups for solid state scientists" by Gerald Burns which is a widely accepted and used book. Professor Richard Hatt, a physics faculty member at BYU-Idaho, did his Ph.D. on solid state physics and was also a source in helping to build crystalline structures for the MIKA program.

## 1.2 Use of PAS

Positron annihilation has the ability to look at the affects of shot peening in Aluminum [3]. This is a process where the metal or sample is compressed by shooting small bb's at the target, creating a compressive stress layer. This makes the distance between atoms a little shorter which will make the material stronger. As the metal heats up it will reach a point where it will undo the affects of shot peening [3].

Professor P.C. Rice-Evans from the University of London used positron beam spectroscopy for the assessment of the structure and defect density of titanium nitride. Many places use positron spectroscopy to probe into a structure to analyze it without damaging the substance. For instance the performance of thin films is largely determined by its microstructure. Because titanium nitride films are used for diffusion barriers for different chemicals and solvents, Professor Evans incorporated PAS to analyze the film. Depending on the project being performed, the film needs to have very little defects. To measure the accuracy of the film deposits, positron annihilation spectroscopy is used to analyze the film down to the microstructure. [4]. The depth of the positron annihilation ranges from  $10^{-7}$ - $10^1$ nm (figure 1.1).

Positron annihilation can recognize different alloys in steels. The increased amount of alloy causes larger grain boundaries which result in an increased lifetime of the

positron. The annihilation will have a lower momentum so the momentum distribution peak will be relatively sharper. Positron annihilation is used when the concentration of defects are very minimal.

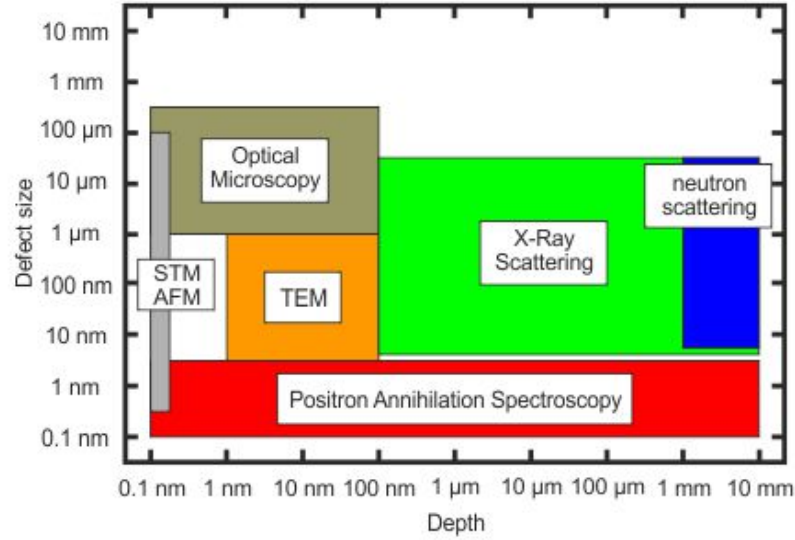


**Figure 1.1** This is a general overview of the ranges of different spectroscopy techniques [4].

### 1.3 Annihilation Background

A positron ( $e^+$ ) is the anti particle of an electron ( $e^-$ ) and they will annihilate each other through an interaction. The annihilation. will result in typically two gamma rays and can be represented as

$$e^+ + e^- \rightarrow \gamma_1 + \gamma_2. \quad (1.1)$$

The total energy of the annihilating pair will be transferred to the pair of  $\gamma$  rays. The energy of these gamma rays is given by

$$\Delta E = \Delta mc^2 + KE \quad (1.2)$$

which is a formula derived from Einstein. The energy will have a specific value since there is a known mass for both a positron and electron. Conservation of energy and momentum both must be conserved and are shown in figure 1.2.

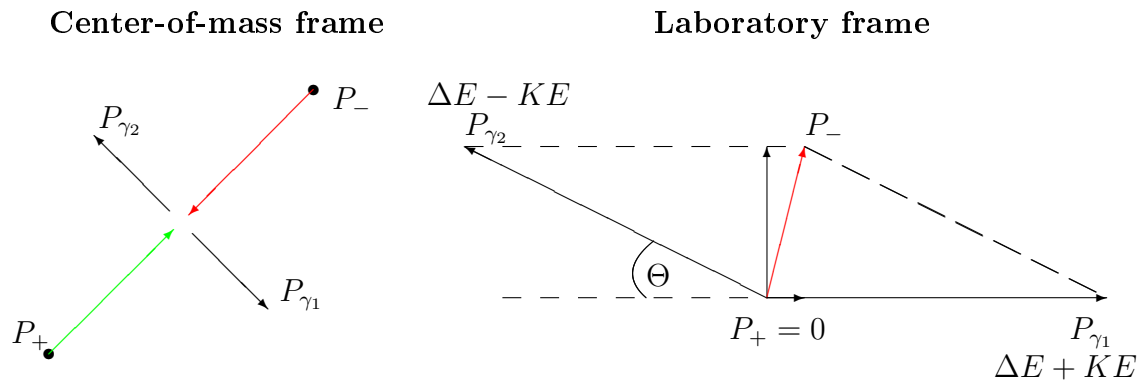


**Figure 1.2** The figure shows what is occurring during an annihilation from two reference frames. The first is from the center of mass where both the electron and positron have the same magnitude of momentum and thus the gamma rays come off directly opposite of each other. The second is from the sitting observer who sees that there is not a momentum from the positron, but rather only from the electron. To conserve both momentum and energy the  $\gamma$  rays will have slightly different energies.

From the laboratory frame, the positron has low momentum in comparison to the momentum of the electron. The momentum is low enough that it is quite negligible and can be treated as zero. Since this is the case, in order to conserve energy the  $\gamma$  ray going parallel to  $P_-$  will have a higher energy than the other  $\gamma$  ray. The higher the momentum, the greater the shift in energy.

For solids with free electrons, such as metals, the positrons will annihilate very quickly. If there are voids in the metal the positron will take longer to annihilate and will have a different amount of energy when it does. The positron will become entrapped in locations where there are defects and thus have a lower probability

of annihilation. The annihilation in this case will most likely occur with a valence electron. The energy difference is due to annihilation with either a valence electron or core electron. The amount of time for this to happen is called lifetime.

Positrons in matter quickly lose energy and live in thermal equilibrium for a short while before annihilating with electrons at a time scale inversely proportional to the electron density. A thermalized positron will generally have a lower momentum, which is why the majority of the contribution will come from the electron. The annihilation will have energy approximately equal to 511 keV. Annihilations that happen with core electrons, indicating fewer impurities will cause energies that experience a greater Doppler broadening from 511 keV, whereas annihilations with valence electrons will produce more  $\gamma$  rays at an energy close to 511 keV.

The graph of gamma ray energies will appear to be a distribution graph. Seeing how spread out the peak is helps to evaluate the solid. This is called the s-parameter. This alone gives no information, but in comparison to other peaks, we are able to understand a lot more.

Both the electron and the positron can be described as a wave ( $\Psi$ ). Since they are a wave, they will have a certain probability of annihilating. The probability ( $P$ ) can be calculated by

$$|\langle \Psi_+ | \Psi_- \rangle|^2 \quad (1.3)$$

or as an integral over all of space,

$$\left| \int_{-\infty}^{\infty} d\mathbf{r} \Psi_+^* \Psi_- \right|^2. \quad (1.4)$$

If the wave functions do not cross at all, this integral will be zero indicating that there is not a possibility of an annihilation. In figure 1.3 there are two gaussian-like wave functions drawn. One representing the electron ( $\Psi_-$ ) while the other is

representing the positron ( $\Psi_+$ ). The probability can be seen as the area under the overlap of the two wave functions. Also, the probability of where it will annihilate will be a gaussian-like distribution. This is just the function inside the integral of equation 1.4.

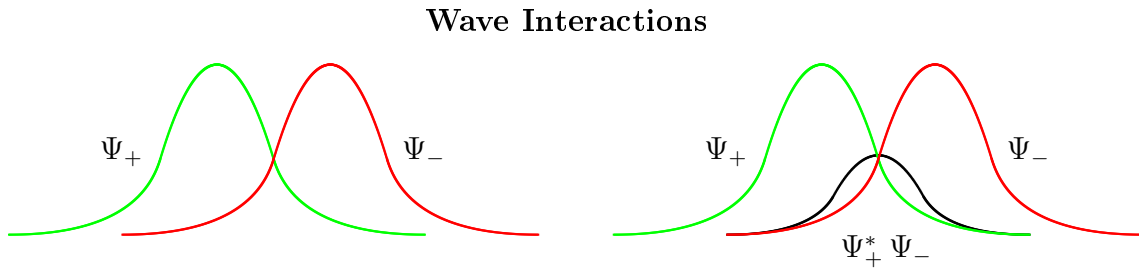


**Figure 1.3** Both the positron and electron are described as waves. How much they interact, or how much overlap the wave functions have, determines the probability of the two wave functions interacting and an annihilation occurs. The probability of where the annihilation will occur is also illustrated.

## 1.4 Crystallography Background

The wave functions discussed earlier are relatively simple to understand. In describing real wave functions they are dependent on space and time ( $\Psi(x, t)$ ). To calculate the wave functions, the location of the nuclei is important. Also, the element that is associated with the electron is equally important to know. To understand the microstructure, a brief background of crystallography will be discussed.

In crystallography, space groups represent and describe the symmetry of a crystal. Think of the symmetry of a human. It could be described as being along a bisecting plane. A cube will have symmetry along many different axis. A crystal is defined as a solid that has uniform chemical composition. The solid is formed with plane faces each making precise angles with each other. Each space group has a different name

and these names help identify their uniqueness.

A point group describes one unit cell and is arranged in three dimensions. It describes the most fundamental structure of a space group. Space groups include translations to form an entire system. The packing efficiency is the fraction of the unit cell actually occupied by atoms. This helps determine the amount of voids that are in a certain crystalline structure. Characters  $a$ ,  $b$ , and  $c$  refer to the length of each side and  $\alpha$ ,  $\beta$ , and  $\gamma$  are the angles. A Wyckoff position is a point belonging to a set of points for which site symmetry groups are conjugate subgroups of the subspace [5].

This thesis involves work with three different space groups. A brief discription of each and their basic symmetries will be mentioned. Different points for each one will be made that will be used later in the thesis.

The cubic is a crystalline structure where the unit cell is in the shape of a cube. One type is a face-centered cubic, which is common among many metals. Examples include gold, aluminum, copper, and silver. Face-centered cubic has atoms at each cubic corner, and one in the middle of every face of the cube. The packing efficiency is relatively high for a face-centered cubic ( $\sim 3/4$ ).

The most common form of ice found on the earth has the space group  $P6_3cm$ . This is called ice  $1_h$  which is included as Appendix A. It is a hexagonal crystal system where  $a = b$ ;  $\alpha = \beta = 90^\circ$ ; and  $\gamma = 120^\circ$ . Figure 1.4 is a water phase diagram which shows the pressure and temperature associated with ice  $1_h$ .

The space group number immediately helps to identify symmetry operations that are going to be in it. In the space group for ice  $1_h$ ,  $P6_3cm$ , the first letter identifies the centering type of cell which is primitive. The  $6_3$  is an 6-fold screw axis. This is a right-handed screw rotation of  $360^\circ/6$  around the axis with a screw vector  $3/6$ . The  $c$  and  $m$  refer to different types of reflections through the plane.

The last space group that will be discussed is from silicon dioxide ( $SiO_2$ ). The

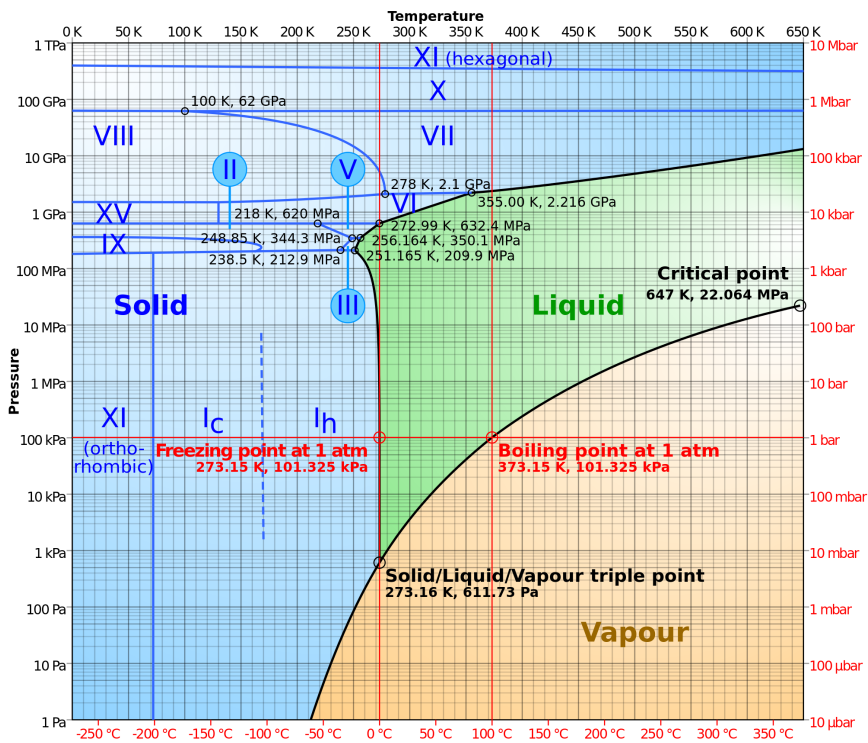


**Figure 1.4** A phase diagram of water is shown. The red horizontal line indicates close to sea level pressures. From this chart it is easy to see that ice  $1_h$  is the most abundant source of ice on the earth. This is the ice type that is modeled. [6]

space group is  $P3_121$  and is trigonal. This comes from the same family crystal family as ice  $1_h$  and has the same restrictions on the cell parameters. The numbers 3, 2, and 1 refer to different translations in the structure. The  $3_1$  follows the same right-handed rotation of  $360^\circ/3$ , but just without a screw vector.

Silicon dioxide actually has two possible space groups:  $P3_121(D_3^4)$  or  $P3_221(D_3^6)$ . The two different groups have similar properties. An equal number of crystals are in both structures, but by observation of the optical rotation of polarized light the two can be identified.  $\text{SiO}_2$  with the space group  $P3_121(D_3^4)$  will rotate the plane of polarization anti-clockwise for light coming towards the observer which is called laevorotatory (this could be possible for other compounds as well).  $P3_221(D_3^6)$  will rotate light clockwise and is called dextrorotatory [7].

The American Mineralogist Crystal Structure Database is a trusted online source for obtaining information on crystals [8]. Along with the name of the space group, it gives the atomic positions of the unit cell. Each one of these will have a different Wyckoff label and from the information from the International Tables For Crystallography, the rest of the atom locations are known.



# Chapter 2

## Method

### 2.1 The Wave Equation

Inside of a solid there are many electrons that are surrounding atoms. Each electron has a unique wave equation. The Kohn-Sham equation is like the Schrödinger equation, but is necessary in describing the wave equation of each individual electron. The equations used are represented in atomic units where  $\hbar = m_e = 1$ . Here is the form of a time-independent Schrödinger equation of a single, non-relativistic particle:

$$E_i \Psi_i(\mathbf{r}) = \left[ -\frac{1}{2} \nabla^2 + V_{\text{eff}}(\mathbf{r}) \right] \Psi_i(\mathbf{r}) \quad (2.1)$$

$$V_{\text{eff}} = V_{\text{ion}} + V_{\text{H}} + V_{\text{xc}} \quad (2.2)$$

The Kohn-Sham equation is unique in that it has an effective potential denoted as  $V_{\text{eff}}(\mathbf{r})$ , which is called the Kohn-Sham potential. The effective potential is comprised of an external potential  $V_{\text{ion}}(\mathbf{r})$ , the Hartree potential  $V_{\text{H}}(\mathbf{r})$  or  $V_{\text{ee}}(\mathbf{r})$ , and the exchange-correlation potential  $V_{\text{xc}}(\mathbf{r})$ . The effective potential is caused from an electron to nuclei interaction. The Hartree potential looks at the interaction approx-

imated by the coulomb potential arising from all the electrons in the system. This is an electron-electron interaction. These both look familiar and are described as,

$$V_{\text{ion}} = - \sum \frac{Qq}{|r - R|}, \quad (2.3)$$

$$V_{\text{H}} = \frac{1}{2} \sum \frac{q^2}{|r - r'|}. \quad (2.4)$$

The negative on the ion interaction is because it will be an attractive potential compared to the electron-electron interaction. To avoid double counting the electron-electron interactions, once the sum is performed it needs to be divided by two. The problem with both of these terms and also with the exchange-correlation potential  $V_{\text{xc}}(\mathbf{r})$ , is that it requires the location of the electrons to be known. In turn, the location of the electrons are yet to be determined from the unsolved Schrödinger equation. This gives need for an alternative way to solve the Schrödinger equation.

## 2.2 Density Functional Theory

There are two theorems that allow the use of density functional theory. The first theorem establishes a relationship between the ground-state energy of the electrons and the electron density. More explicitly it states that the ground-state energy is a unique functional of the electron density [9]. A functional is a function of another function. It is specified by square brackets around the inside function. For example the exchange-correlation energy is represented as  $E_{\text{xc}}[n(\mathbf{r})]$  (equation 2.9).

The second theorem states that the density which minimizes the total energy is the density associated with the ground-state wavefunction. So by finding the density which minimizes the energy as much as possible, this will be the density related to the ground-state of the system. Proof of these two theorems are left up to the reader.

The electron density is a function of space and time. From the theorems above, if the system is not changing the electron density will be constant through time. The assumption is made that the system is not changing; therefore, the electron density distribution is calculated from the probable location of all the wave functions. This is represented as

$$n(\mathbf{r}) = \sum_i^N |\Psi_i(\mathbf{r})|^2. \quad (2.5)$$

A sample of the electron density for copper is shown in figure 2.1. The strongest part of the electron density should be around the nuclei.

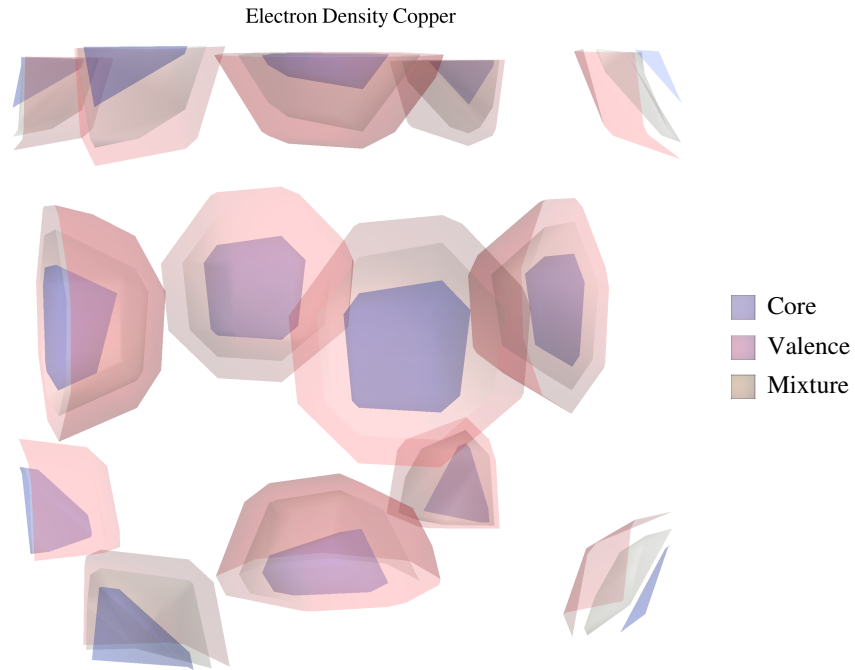


**Figure 2.1** This is a primitive cell of copper. The electron density is shown on different contour levels. These are stronger or more dense as we get closer to the ions.

The electron density is obtained by summing over all the electron wave functions and finding the probability where each one is located. The exchange-correlation potential is based from the Pauli Exchange Principle which states that two electrons

that have the same spin cannot be in the same place at the same time. This will cause a repulsion between electron of the same state. Letting  $e = 1$ , each effective potential can be represented as

$$V_{\text{ion}} = - \int \frac{n(\mathbf{r}')}{|\mathbf{r} - \mathbf{r}'|} d\mathbf{r}', \quad (2.6)$$

$$V_{\text{H}} = \int \frac{n(\mathbf{r}')}{|\mathbf{r} - \mathbf{r}'|} d\mathbf{r}', \quad (2.7)$$

$$V_{\text{xc}} = \frac{\delta E_{\text{xc}}[n(\mathbf{r})]}{\delta n(\mathbf{r})}. \quad (2.8)$$

In the MIKA program the local-density approximation (LDA) is used in finding the exchange-correlation energy. An LDA does exactly what it sounds like it should do and this is done by

$$E_{\text{xc}}[n(\mathbf{r})] = \int \epsilon_{\text{xc}}(n(\mathbf{r})) n(\mathbf{r}) d\mathbf{r}. \quad (2.9)$$

In order to solve the exchange-correlation potential it is simple to approximate using a taylor series expansion. After two terms the value becomes extremely negligible so the first two are all that will be used. The exchange-correlation potential then becomes

$$V_{\text{xc}}(\mathbf{r}) = \epsilon_{\text{xc}}(n(\mathbf{r})) + n(\mathbf{r}) \left. \frac{d\epsilon_{\text{xc}}}{dn} \right|_{n=n(\mathbf{r})}. \quad (2.10)$$

Both the Hartree potential and the ion potential can be solved by taking the gradient of each one. If the gradient were done in three dimensions, it would properly explain how the potential drops with respect to some distance. These potentials can be solved from the Poisson equation

$$\nabla^2 V_H(\mathbf{r}) = -4\pi n(\mathbf{r}). \quad (2.11)$$

For the Hartree potential the electron density  $n(\mathbf{r})$  is replaced with the total charge density  $\rho(\mathbf{r})$ . A positive gaussian charge is placed at the center of the ions to neutralize the system. After equation 2.11 is solved for the total charge density the potential from the positive gaussian charge is replaced with a pseudopotential. A pseudopotential is used to approximate the actual potential. From figure 2.2 there exists a certain cutoff region  $r_c$  where both potential and wave functions match with pseudo waves and potentials.

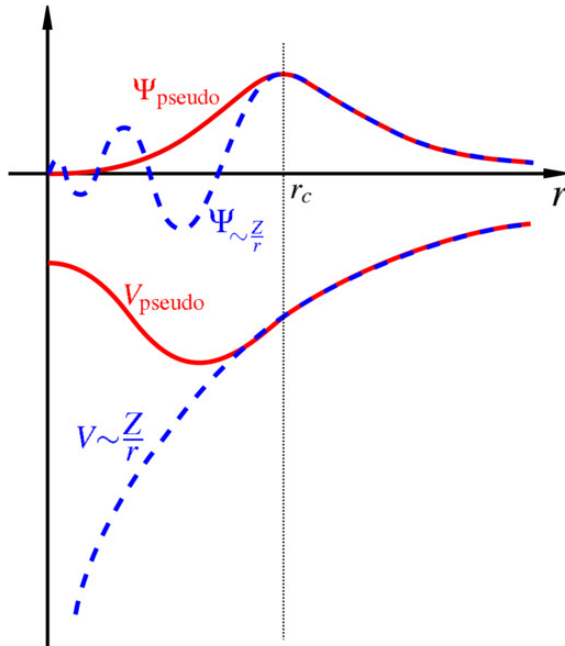


**Figure 2.2** This is a comparison of the wave function and potential to the pseudopotential and pseudowavefunction.

The total energy of the system can then be written as

$$E_{\text{total}} = \sum_i^N \int \Psi_i^*(\mathbf{r}) \left( -\frac{1}{2} \nabla^2 \right) \Psi_i(\mathbf{r}) d\mathbf{r} + \frac{1}{2} \int V_H(\mathbf{r}) n(\mathbf{r}) d\mathbf{r} \\ + \int V_{\text{ion}}(\mathbf{r}) n(\mathbf{r}) d\mathbf{r} + E_{\text{xc}} + E_{\text{ion-ion}}, \quad (2.12)$$

where the  $E_{\text{ion-ion}}$  is the repulsive interaction between the nuclei of the system. If the density is found that will bring the total energy to it's minumum, then that density will correspond to the ground-state of the system which was discussed earlier.

It is also worth noting that a similar process could be done including the positron density ( $n_+(\mathbf{r})$ ). Equation 2.13 is similar to how the electron density was calculated. For the positron density however,  $N_+ = 1$  because only one positron needs to be considered. The same processes in solving the Kohn-Sham equations are observed only there will be slight differences with signs on potentials. The positron density is represented as

$$n_+(\mathbf{r}) = \sum_i^{N_+} |\Psi_i^+(\mathbf{r})|^2. \quad (2.13)$$

A sample of the positron density for copper is shown in figure ?? . The positrons will be repelled by the ions so the strength of their locations should be as far away from the ions as possible. It is also easy to see that the previously vacant areas in figure 2.1 (the electron density) is now the occupied areas by the positron density. This is exactly what is expected.

## 2.3 Multigrid Methods

The meaning of MIKA, Multi-grid Instead of K-spAce, indicates the use of multigrid methods. These methods are used to solve the electron density of the ground-state energy. A multigrid method can incorporate many different algorithims for solving

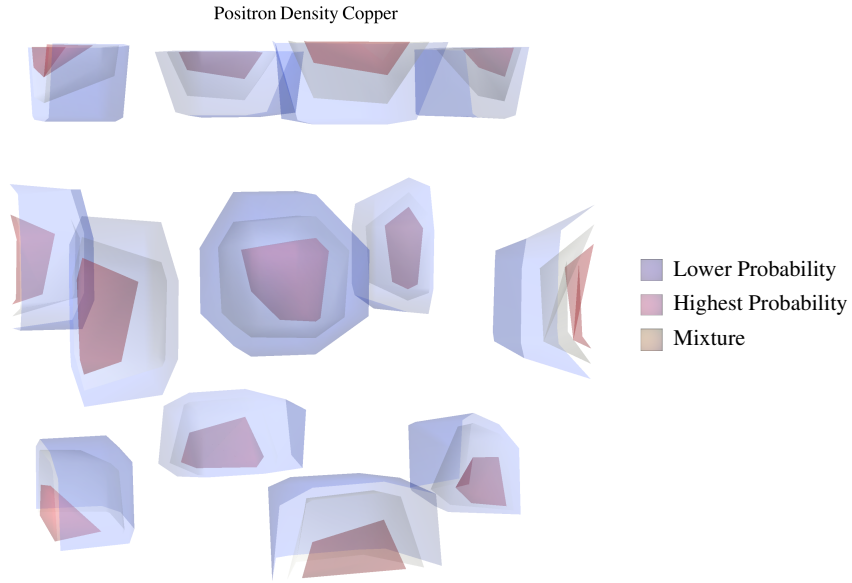


**Figure 2.3** This is a primitive cell of copper. The positron density is shown on different contour levels. These are stronger or more dense as we get further away from the ions.

differential equations. That is essentially what is present. To solve the previously discussed equation requires that we know the electron density; yet, the electron density is calculated from our wave functions. This is a differential equation.

A basic method that would solve the differential equations is called the Jacobi method. Mathematically the Jacobi method can be expressed as

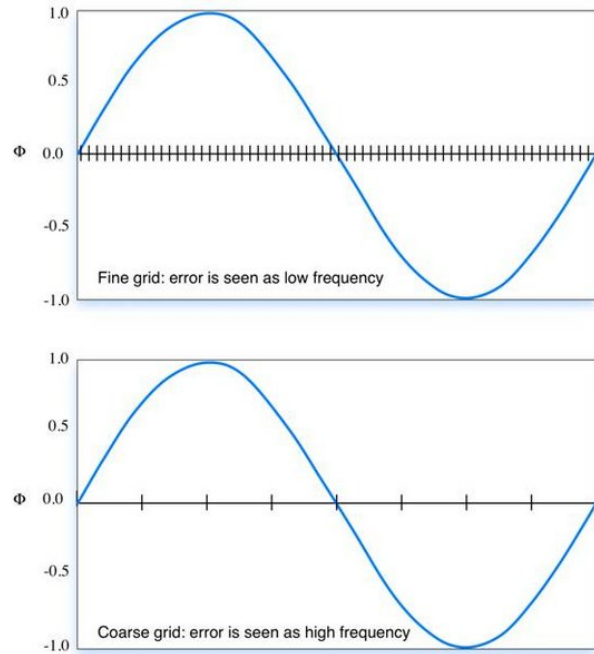
$$V_{\text{new}}(i, j) = \frac{1}{4} [V_{\text{old}}(i + 1, j) + V_{\text{old}}(i - 1, j) + V_{\text{old}}(i, j + 1) + V_{\text{old}}(i, j - 1)] \quad (2.14)$$

in a two dimensional system. This is a relaxation algorithm that evaluates old values that surround the new value and takes the average of them. This sweep continues multiple times until the system no longer changes. The only problem with this method is that over time it would introduce a critical slowing-down phenomenon (CDS). This method uses information from the local surrounding areas during each pass (local order of approximation). So any immediate differences will be reduced; however,

once it has been reduced the slow convergence dominates the overall error reduction rate, i.e. CSD occurs [10].

The convergence rate of standard relaxation solvers seems to stall after just a few passes. These solver are much better on a coarser grid. During a pass the information travels in one direction, one grid unit at a time. To have proper convergence the information needs to travel back and forth numerous times. For many different methods, the number of passes to reach a convergence is linearly proportional to the number of nodes in a specific direction. To take advantage of this, multigrid methods will define a coarser grid where the low frequency will be seen as a high frequency (figure 2.4).

**Figure 2.4** Multigrid methods will define a coarse grid that the low frequency will be seen as a higher frequency. Implementing multigrid techniques will increase computation time and reduces a slow convergence. To transfer from one grid to another requires an operator: Restriction to go from fine to coarse, and Prolongation to go back to a fine grid.



The main idea of multigrid methods is to use multiple different types of algorithms: some that are more localized (fine grid) and others that are more generalized (coarse grid). The process of going from one grid to another is called Agglomeration. A Restriction operator is an interpolation method to go from a fine grid to a coarser grid. So it takes a function on a fine grid and produces the function on a coarse grid.

A Prolongation is just the inverse. Going to a coarser grid requires a call back to the original fine grid (figure 2.5).

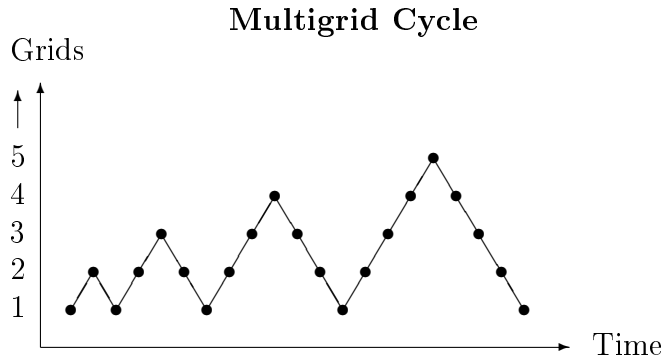


**Figure 2.5** Each call to a coarser grid needs to pass through all the grids leading up to that grid. This is often referred to as a V or W for apparent reasons.

MIKA doppler uses a customized version of the Rayleigh quotient multigrid method (RQMG). The first and simple relaxation method is called a coordinate relaxation. This uses techniques very similar to the Jacobi method only by solving a discretized eigenproblem. This will suffer from CSD because of the local order of approximation. A coarse grid will then substitute the fine grid by

$$u'_f = u_f + \alpha I_c^f e_c. \quad (2.15)$$

The subscripts  $f$  and  $c$  stand for the fine and coarse grids and  $I$  is the prolongation operator that interpolates between the two grids. For the finest grid a Gauss-Seidel method is used and converges to the nearest eigenvalue, which is as expected.

The Hartree and exchange-correlation potentials are evaluated on the finer grid. To return to the coarse grid, density function will be represented as

$$n_f = \sum_i |I_c^f \Psi_{i,c}|^2. \quad (2.16)$$

Once the output density  $n_{out}$  is obtained, it continues through an iteration until  $n_{out}$  is equal to  $n_{in}$ . In large systems this may take a long time so a degree of precision can be entered by the user to determine the accuracy.

## 2.4 Annihilation

Now that the electron density and positron densities are known, the annihilation rate can be calculated. The annihilation rate is best understood using the most simple case. Equation 1.3 describes the probability of the overlap of the two wave functions.

Breaking up this equation yields

$$\langle \Psi_+^* | \Psi_- \rangle \langle \Psi_-^* | \Psi_+ \rangle, \quad (2.17)$$

which is seen as an integral of the wave functions over all of space,

$$\int \int d\mathbf{r} d\mathbf{r}' \Psi_+^*(\mathbf{r}) \Psi_+(\mathbf{r}') \Psi_-^*(\mathbf{r}) \Psi_-(\mathbf{r}'). \quad (2.18)$$

For the exchange-correlation energy (equation 2.9) a local density approximation (LDA) was used. In the crystalline structure the electrons are close to each other so the LDA is appropriate to incorporate. Once the LDA is used in equation 2.18 it becomes

$$\int d\mathbf{r} |\Psi_+(\mathbf{r})|^2 |\Psi_-(\mathbf{r})|^2 \delta(\mathbf{r} - \mathbf{r}'). \quad (2.19)$$

The annihilation rate, represented as  $\lambda$ , is almost complete. In order to have a probability of interaction, a cross section is needed. For the radius of the cross section, the classical electron radius  $r_0$  will be used. The speed at which positrons enter the system can be thought of as an intensity and will be called  $c$ , or the speed of light. The annihilation rate for one electron and one positron can be observed as

$$\lambda = \pi r_0^2 c \int d\mathbf{r} |\Psi_+(\mathbf{r})|^2 |\Psi_-(\mathbf{r})|^2 \delta(\mathbf{r} - \mathbf{r}'). \quad (2.20)$$

Whereas the annihilation rate over all the electron and positron wave functions is calculated by the summation

$$\lambda = \pi r_0^2 c \sum_i^N \int d\mathbf{r} |\Psi_i^+(\mathbf{r})|^2 |\Psi_i^-(\mathbf{r})|^2 \delta(\mathbf{r} - \mathbf{r}'). \quad (2.21)$$

The summation and integration are interchangeable so the summation will go right to the wave equations. After recalling equation 2.5, it is easy to see the process by which MIKA calculates the annihilation rate. This is seen by

$$\lambda = \pi r_0^2 c \int d\mathbf{r} n_+(\mathbf{r}) n_-(\mathbf{r}) \gamma(n_-(\mathbf{r})). \quad (2.22)$$

The enhancement factor  $\gamma$  replaces the dirac from equation 2.21 and takes into account the pile-up of electron density at the positron due to a correlation affect [2]. The electron and positron density can be thought of as a particle density or particles/ $m^3$ . It is now easy to see that the integration the equation yields units of  $1/s$  which is as expected. The inverse of the annihilation rate is the positron lifetime,  $\tau = 1/\lambda$ .

## 2.5 Simulation

To help understand the process of annihilation a matlab code was written to simulate basic interactions with a positron-electron pair. Instead of doing a multi-wave problem where the positron and electron densities are preferred, I kept it as a simple one dimensional positron and electron wave.

The goal was to re-create figure 1.3 using the function inside the integral of equation 1.4. This time I created it computationally rather than theoretically. I also

wanted to move the positron wave packet and calculate the probability of overlap and the basis of annihilation from equation 1.3. The results are seen in figure 2.6.

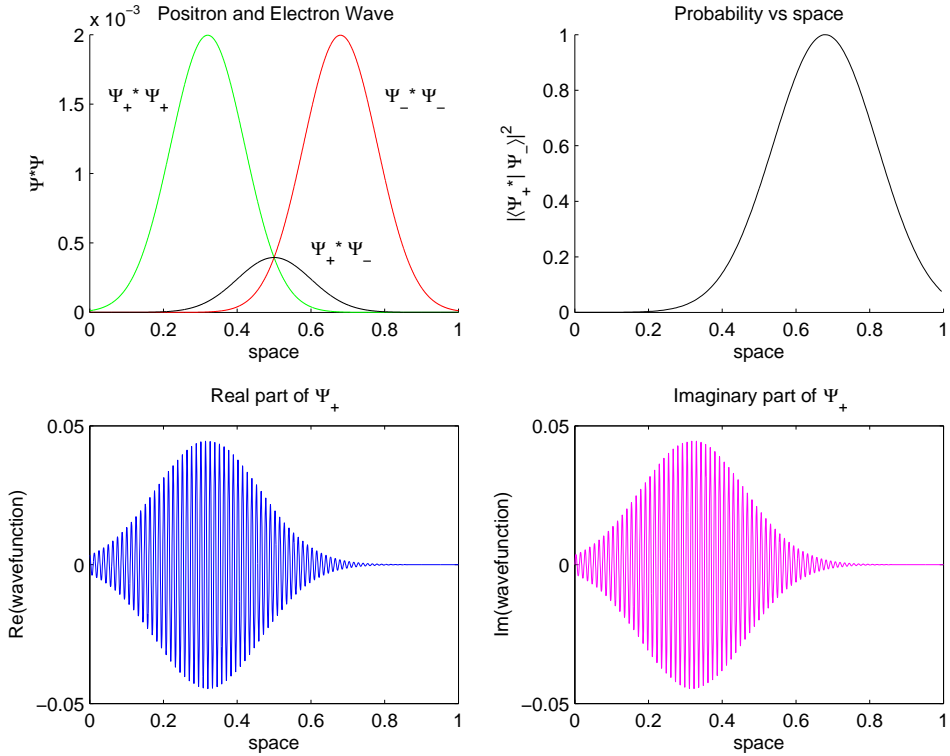


**Figure 2.6** The graph in the top left is a computational re-creation of figure 1.3. The top right graph shows the probability of an interaction of the positron and electron pair. The electron was stationary as the positron moved in space to all locations, giving a probability through space. The bottom right and left graphs are the real and imaginary parts of the positron wave function.

While representing the positron-electron pair, there were a few variables that were distinct. The wave functions are time independent and so was the energy. The momentum of both waves were also the same. Representing the annihilation rate and positron lifetime is relatively simple from this point as shown in figure 2.7.

The electron is stationary while the positron moves to calculate the annihilation rates and lifetimes throughout space. The location of the electron is the same as the top left graph in figure 2.6. To give an idea of where a pure sample of copper would be on these graphs, the location is made known. Also, the lower two graphs show the

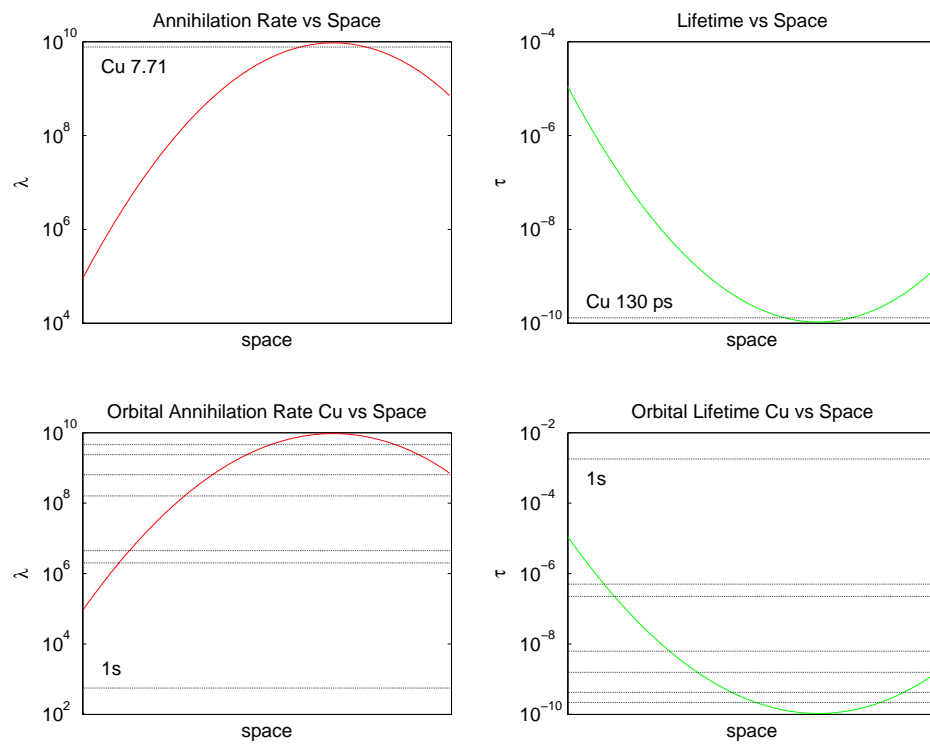


**Figure 2.7** The graph on the top left is the annihilation rate. The electron was stationary as the positron moved in space to all locations, giving a probability through space. The top right graph shows the lifetime through space of the positron and electron pair. The bottom right and left graphs are the same graphs as above, only with the actual computed orbital rates and lifetime from a pure copper sample.

same as the top, but just with all the orbitals included. Only the 1s shell is labeled as the reader can readily identify the others.

The graphs were generated from a one dimensional system, whereas the copper information is from a three dimensional system using discrete data. Because of this the comparison will not be exact, but it can be used to show simple illustrations. From the graph in the bottom corner the 4s shell has the highest annihilation rate, and therefore is closer to the positron. The 1s shell has the smallest annihilation rate meaning that the electron and positron are far from each other. As vacancies are introduced into the system the positron wave function will be more likely to go to

that region causing it to be further away from the 1s shell. Thus it would lower the overall annihilation rate and increase the lifetime of the positron.

# Chapter 3

## Procedure

### 3.1 Crystalline Structure

The basic symmetry of copper, ice 1<sub>h</sub>, and silicon dioxide were discussed earlier. The actual making of a supercell becomes quite a tedious process. In order to run the MIKA doppler program, a data file that has the position of all the atoms in the cell must be made. MIKA will only understand coordinates in the cartesian coordinates with  $\alpha = \beta = \gamma = 90^\circ$ . Systems without this need to undergo a coordinate transfer (ice 1<sub>h</sub> and SiO<sub>2</sub>).

The coordinate transfer from ice 1<sub>h</sub> or SiO<sub>2</sub> is relatively straight forward. Figure 3.1 shows the visual transfer along with the mathematical representation of the transfer. The new coordinates now have a possibility of having a negative x value, so a statement should be set to catch the negative values. Once a negative is detected, simply adding one lattice length to the number will get it back in the correct position.

For convenience and times sake, I made a program called coordtranslate. This program eventually was made to have two purposes: to translate coordinates into a complete orthonormal basis, and extend the unit in multiple directions for supercells.

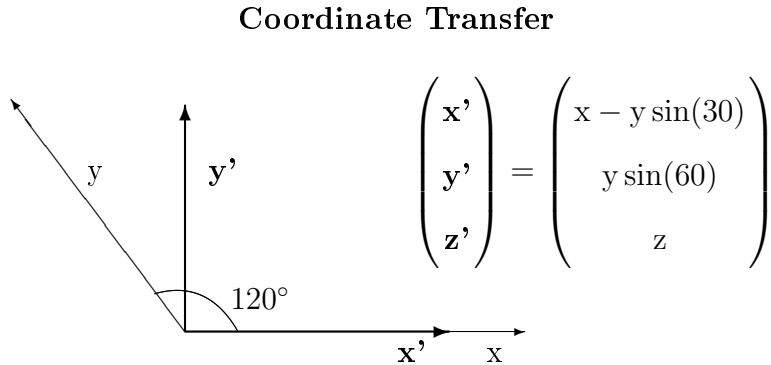


**Figure 3.1** The MIKA Doppler program needs the coordinates with  $\alpha = \beta = \gamma = 90^\circ$ . This is showing the basic undergoing of that transformation.

Care was taken during the extending into the supercell to keep the symmetry the same. The output of coordtranslate would put it in the format that MIKA required. This comprised of <atom type> <current atom count> <x> <y> <z> <0.0> (Appendix B). The last input is to indicate to the program that this atom's information is done.

Coordtranslate has three parameters taken from the user. The first is the location of the atoms in the unit cell. This was stored in another file in a three column format representing x, y, and z coordinates. The second is whether it needs to translate it into orthonormal basis (understood by the number 1) or whether it is already orthogonal (2). The last is how big to make it: 1 meaning one unit cell, 2 meaning two unit cells, etc. Input files with over 900 atoms were made in seconds using this program.

## 3.2 INPUT

Once the crystalline structure has been made, it needs to be put in the MIKA program in the proper place with the needed attributes. SiO<sub>2</sub>\_bulk\_9, a pure silicon dioxide

containing nine atoms is included as Appendix B. This is called an INPUT file. It is located in the MIKA/doppler/MIKADoppler\_user/WORK/START file and is given a name such as SiO<sub>2</sub>\_bulk\_9. The name needs to be distinguishable as other files will be generated in other folders with the same name.

Great care must be taken in the INPUT file. The sixth line tells the MIKA program the elements that are being used. The element name points MIKA to a file found in the /MIKADoppler\_user/FREE\_AT\_IN/atominput/ This is used to construct the free atom wavefunction for each atom that is present in the system. In this folder there are twenty four of the more commonly used elements. If the user wishes to model an element that is not found in this folder the user must build a file to represent that element. Further help for the INPUT file can be found in Appendix B.

The program is started from the MIKADoppler\_user folder by the command ./doppler\_4Par WORK/START/<INPUT>. If the INPUT file is correct it should only take a few seconds to complete. Three files are made from the program. Annihilation rates are stored in /MIKADoppler\_user/DATA/RATES/<INPUT>, momentum distributions are found in /DATA/M\_DISTR/<INPUT>, and the decomposed momentum distributions are in /DATA/DECOMP/<INPUT>. Located in the /MIKADoppler\_user/atsup99\_wrk folder are OUTPUT files which have electron densities, positron densities, and potential. The results in the /atsup99\_wrk folder are not stored automatically and are overwritten on the next run.

In the /atsup99\_wrk folder is found a file called atoms.xyz The file can be opened in gOpenMol which is easily found on the internet and is an open source package. This program will take the file atoms.xyz and plot them in three dimension (see figure 3.2). This is extremely helpful to the user as a check that the lattice structure is correct and symmetries are observed as expected.

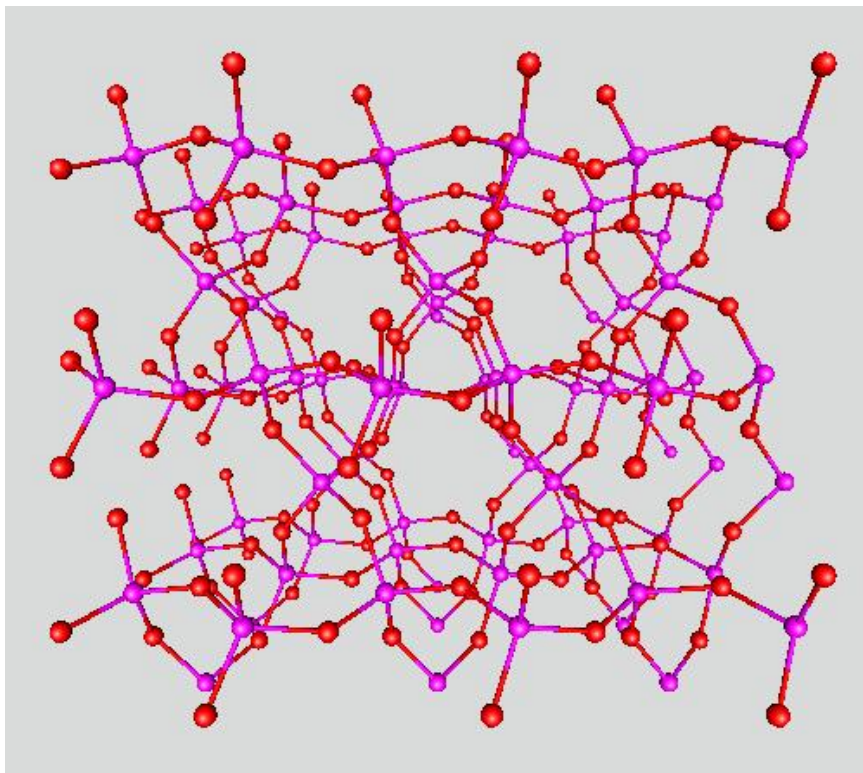


**Figure 3.2** This is a silicon dioxide ( $\text{SiO}_2$ ) crystalline structure. It is a supercell that has 243 atoms: 81 silicon and 162 oxygen. On the second page of Appendix A., it describes the symmetry that should be observed. Seeing the symmetry that should be observed gives strong evidence that the procedure was correct in building the system.

### 3.3 Manipulation

The electron densities and positron densities are in a three tiered loop. The first value is where  $x=1$ ,  $y=1$ , and  $z=1$ . The  $x$  value will then increase up to the grid size and start back over now with  $y=2$ . This continues ( $\text{grid points}$ )<sup>3</sup> times so that every point has a density. With the help of Professor Kevin Kelly, a program was made called translate. The program is run by `./translate <file> <grid points> <new file name>`. Grid points is a parameter that is used on the INPUT file. The output from translate is in the format  $(X,Y,Z,W)$  where  $W$  is the value at the given location. From this point gnuplot or another source can be used to plot the file.

The files in /M\_DISTR/ are comprised of the total momentum distribution. MIKA will output the files in units of  $m_0c$ . To manipulate this data I built a program called convolution. This has many features which are used mostly to compare with experimental data. The program is run by <convolution> <file> <function>. The function comprises of four different options. <s> refers to the s-parameter and must be followed by an integer specifying how many channels over it should calculate. It will return the s-parameter. <w> refers to the w-parameter and must be followed by two integers to specify the begining and end of the parameter. It will return the w-parameter. <p> will print the counts normalized. <e> will take the file and convert the momentum into the energy based around 511keV and the print will be normalized.

The momentum distribution still needs to be operated on by a convolution. In functional analysis, convolution is a mathematical operation on two functions, producing a third function that is typically viewed as a modified version of one of the original functions. Convolutions have their place in many fields including science, engineering, and mathematics.

In figure 3.3 it shows a momentum distribution of a bulk copper with and without a convolution. The momentum distribution is convoluted with a gaussian. It takes the file and uses the full width at half maximum (FWHM) to produce the gaussian, by which it is then convoluted. This is an extremely common practice and is an approved method. From the figure, the convoluted curve is much smoother than the original curve. This better reflects data that will be taken in the laboratory.

The decomposition of the momentum is useful in detecting which shell is more probable at different momentums in annihilation. In the INPUT file the user decides how many shells will be represented in the decompostion output. In all of the calculations that were done, all the electron shells were represented. Figure 3.4 shows a

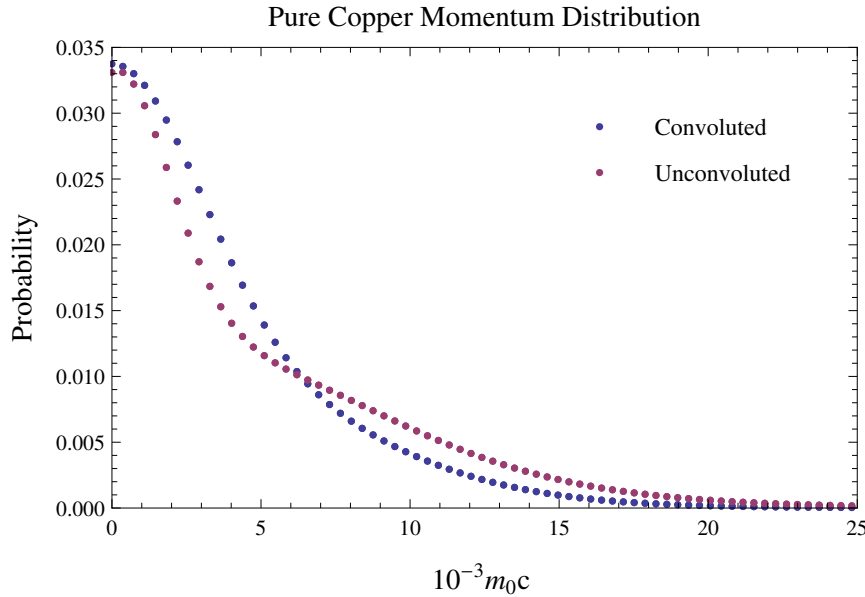


**Figure 3.3** This is a pure primitive cell of copper. MIKA will output the unconvolved line and for realistic means it is convoluted. This is done with a gaussian that is made from FWHM of the unconvolved data.

copper bulk sample that has decomposed momentum distributions.

Figure 3.4 also helps to visualize why the peak in figure 3.3 would be sharper with more defects. The more defects a system has, the more likely the positron will become caught in a vacancy. This will then have a higher probability of having an annihilation with an valence electron. From the distribution, the valence electron will most likely have a lower momentum, so the overall peak on the momentum distribution will be higher.

The opposite is also true. With less defects the positron will be closer to the core electron, even though they will still have a higher probability of annihilation with a valence electron, and therefore have a higher probability than normal of annihilation with a core electron. This will result in a higher momentum so the peak will be lower and the base will be more spread out.

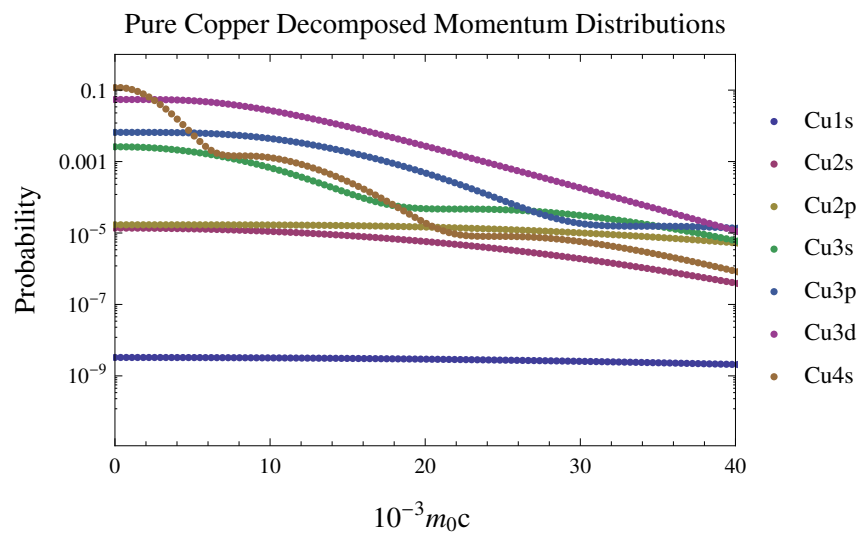


**Figure 3.4** This is a pure primitive cell of copper. This breaks the momentum distribution (figure 4.3) down into each part: 1s, 2s, 2p, etc. The probability on the left is on a log scale so as to see the spread between all the different levels.



# Chapter 4

## Copper

### 4.1 Copper Pure

John Barrett, a graduate of Brigham Young University Idaho, was able to model pure copper and copper with vacancies. The first goal in this thesis was to duplicate and learn from his work. His data matched with raw data which helped affirm the validity of his research.

In trying to understand where the positron will annihilate with an electron, it is interesting to plot the electron density with the positron density (figure 4.1). The outer valence shell of the electron density is shown in red and the positron density is in green. To obtain a middle ground between the two, representing a possible annihilation location, I plotted a contour of the differences. This is seen as the blue contour. This is not exactly accurate because the probabilities of all the electrons, including the core, will produce a probability that is closer to the electron density than the positron density.

Since copper is a face-centered cubic it has an incredible amount of symmetry. An easy and effective method of seeing if we are correct is if the density of both electron

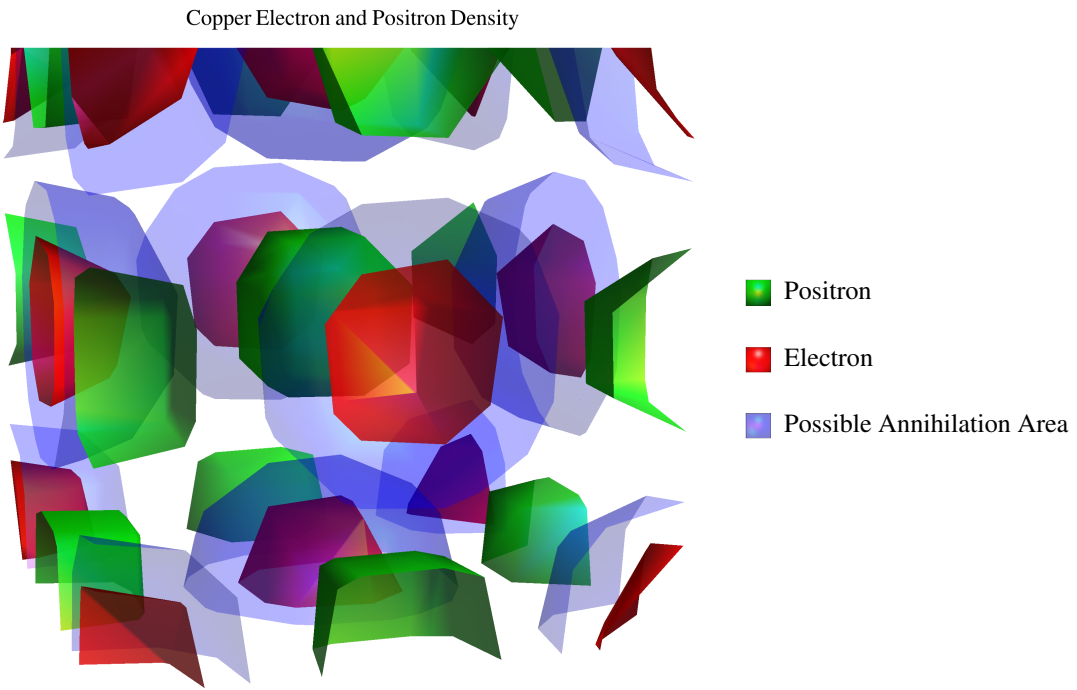


**Figure 4.1** This is a primitive cell of copper. The electron density is in red and the positron density is in green. The middle location between the two would be a probable location of annihilation and is shown as blue. The actual probability location of annihilation will be closer to the electron density.

and positron show a specific and reasonable pattern. The figure shows exactly what would be expected. As vacancies or defects are added, it is useful to recall back to figure 4.1 to notice how the densities have changed and why they have changed.

The first step is to compare the results from computational to the results that are given experimentally. This is shown in figure 4.2. Both results have been normalized and it is incredible to see how closely related the two graphs are to each other. This helps give immediate reassurance that the computational process and results are accurate and useful.

This graph will be a good comparison for when impurities and vacancies are introduced into the system. The S parameter will be taken by adding the area under the curve from zero to the line that has been indicated. This does not matter exactly

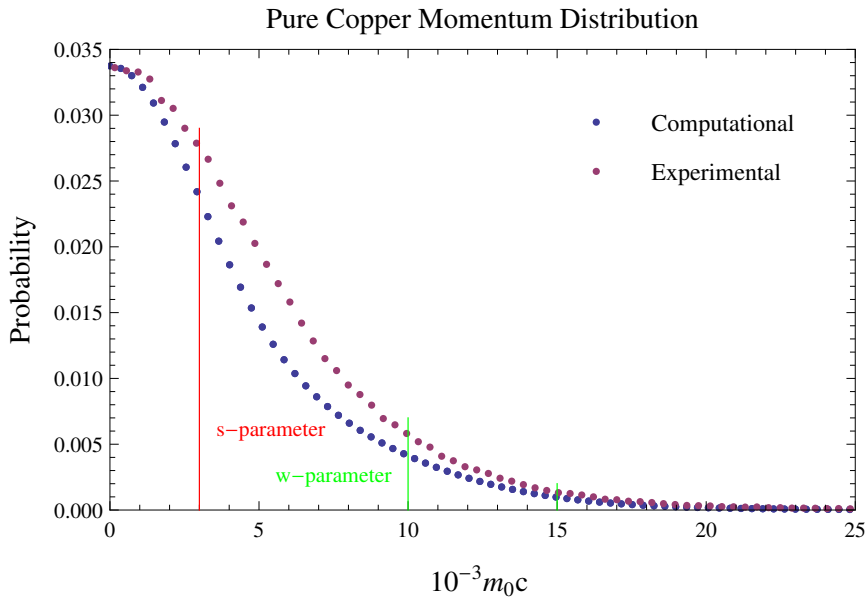


**Figure 4.2** This is a momentum distribution of a pure sample of copper with experimental and computational results. Once the computational results have undergone a convolution, the results are similar to experimental. The convolution was performed using a FWHM gaussian. The curve is similar and with further research, a more accurate convolution could be calculated.

where, only that we are consistent with every single measurement of copper after this. The wparameter is calculated by adding the area under the curve from the two locations.

When comparing the S and W parameters it is important to have a constant, or something that can be a reference. In the following two sections vacancy and defects will be introduced. Some of the density pictures may be shown with just the primitive cell, but the s and w parameters will be calculated from a supercell of four primitive cells.

The decomposed momentum distribution for this pure sample is shown in figure 3.4. It should also be used as a reference point in observing why vacancies would produce a sharper peak in the momentum distribution.

## 4.2 Copper Vacancy

Now it is time to introduce a vacancy into the system and notice how it changes. This is done by building a supercell of 32 copper atoms. An atom will be located at the very center, so this is the atom that will be removed so it is easy to see the affects it has on nearby ions and electrons.

Plotting the electron density did not show anything extremely interesting; however the positron density highlights a few interesting observations. In figure 4.3 the positron density is plotted, but only one level of it. Adding more levels to the plot made it harder to interpret.

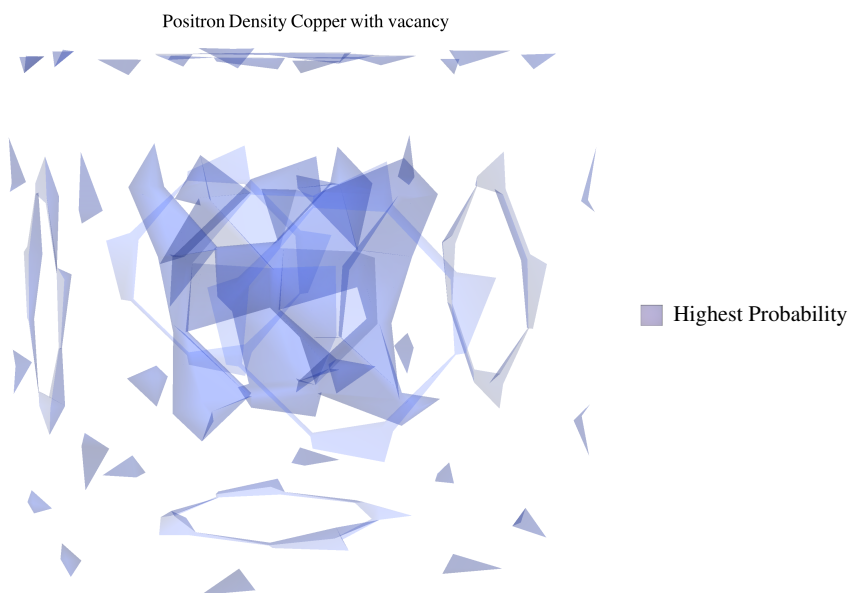


**Figure 4.3** This is a supercell of copper that has one vacancy in the middle of it. The vacancy causes the ions around it to also flex a little, which is why the positron density shows symmetry in these areas affected by flexing ions.

Due to the absence of an ion, the ions are going to shift ever so slightly. This was apparent as I noticed it took four more calculations of the Rayleigh quotient multigrid, indicating that there was a greater change than originally. The symmetry around the vacancy and to the edge of the supercell shows that the electrons did flex

towards the vacancy.

### 4.3 Copper Defects

To keep with consistency, a supercell will be taken and an impurity will be added to the center of one of the primitive cells. This will not produce the center symmetry, like in figure 4.3, because it is off center. To help show the actual symmetry, a hydrogen atom is added to the center of a unit cell and plotted in figure 4.4.

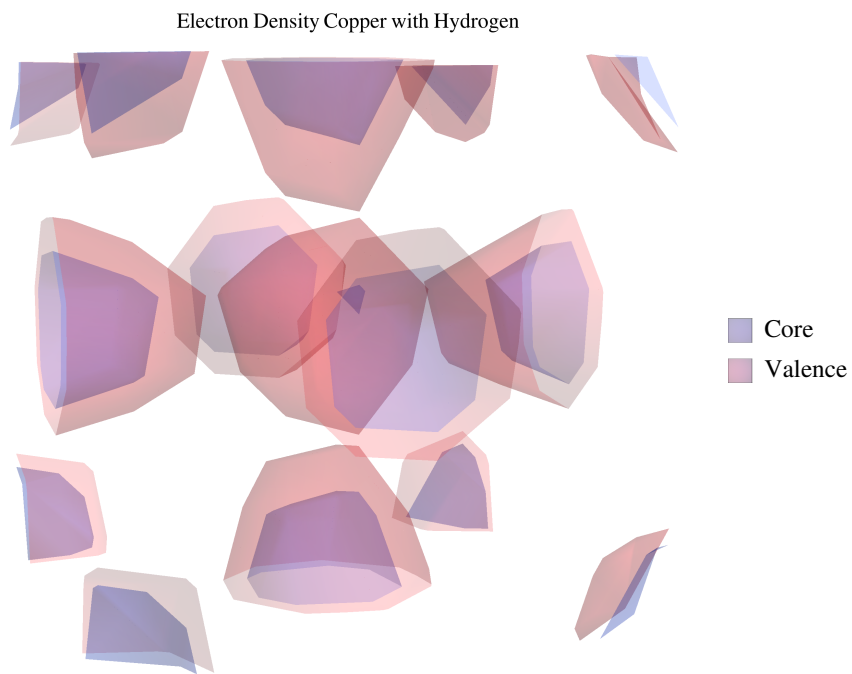


**Figure 4.4** This is a primitive cell of copper that has one hydrogen atom in the middle of it. The hydrogen atom causes there to be a slight concentration of electron density in the middle where it was void before.

In comparing figure 4.4 with figure 2.1, the electron density has intensified a little. This is apparent in the side electrons that are now skewed a little from what they were previously.

For the actual comparison, an oxygen molecule was used. This was partially

because a hydrogen showed zero difference out past what I would consider an uncertainty. For 32 atoms the difference was in the seventh significant figure.

Figure 4.5 shows the positron density of a primitive cell with a hydrogen atom in the center. The original primitive cell had a strong electron density in the center and after placing a hydrogen atom in the middle it completely eliminates the positron density that was there.

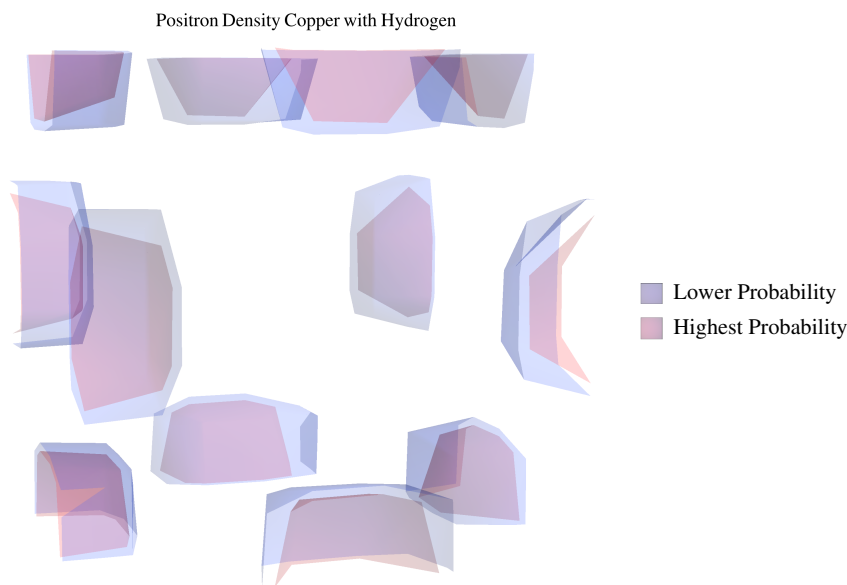


**Figure 4.5** This is a primitive cell of copper that has one hydrogen atom in the middle of it. Because of the hydrogen molecule, the positron is repelled to the outer regions.

## 4.4 Copper Analysis

Looking at the electron and positron densities are very interesting, but need to be compared to something that we can actually measure in a lab. This is the momentum distribution. Figure 5.1 shows all three comparisons without a convolution.

There is a sharper peak on the sample that has a vacancy. This is exactly what

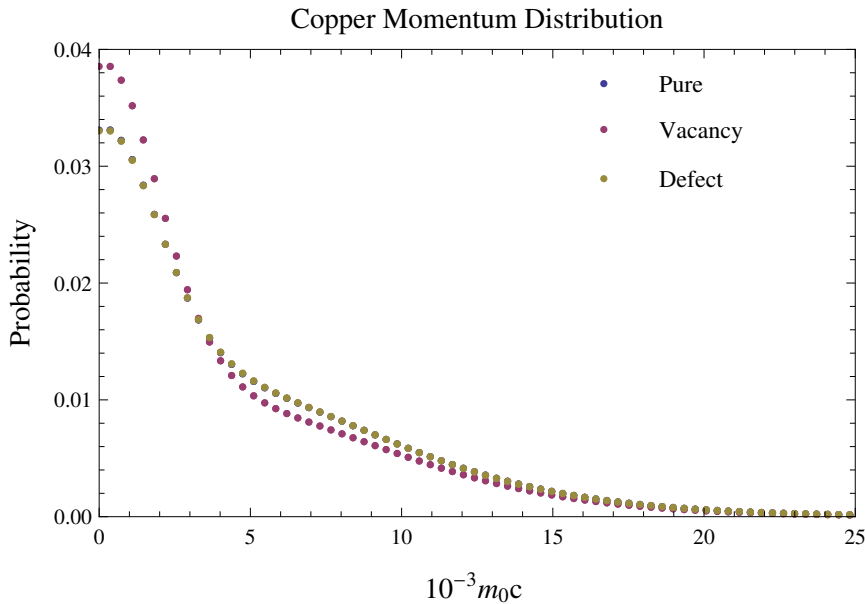


**Figure 4.6** This is a momentum distribution of copper with a pure sample, one vacancy, and one defect. The defect is an oxygen and it runs almost exactly with the pure sample.

should be noticed. That implies that the positrons annihilated with more valence electron than in the pure sample. The pure is hard to see because it runs almost exactly with the defect sample. The defect was an oxygen so there are six more electrons introduced into the system, which is not many compared to the entire system. This is the reason why the two lines are almost exact.

The table in figure 4.7 shows the S and W parameters of these different copper samples. The S and W parameter locations are kept the same, so the only difference is the function or area underneath the curve. The detectors at Brigham Young University-Idaho have an uncertainty out in the third decimal place. According to this and what has been recorded, the detectors would not notice a difference between a pure sample and a sample with one oxygen defect in it.

Copper sample	s-parameter	w-parameter
Pure	.492	.154
Vacancy	.551	.134
Oxygen defect	.492	.154
Experiment pure	.495	.155
Experiment defects	.493	.153

**Figure 4.7** The copper sample used in computation is a super cell comprised of four primitive cells. Introducing only one oxygen will not have enough affect that will be observable. For the experimental data with defects, a pure sample was taken and sand paper was applied to introduce impurities. Further computational research needs to be performed to predict what impurities are the sample.

# Chapter 5

## Ice 1<sub>h</sub>

### 5.1 Ice Pure

Ice, unlike copper, does not have a very symmetric primitive cell. The electron and positron densities are a little harder to visualize. Figure 5.1 is the electron density in ice 1<sub>h</sub>. Upon first glance it does not appear to be correct. There appears to be two layers that comprise an electron density. This is not what has been observed thus far in copper because it does not have uniform symmetry.

It has already been discussed that the packing efficiency of ice is relatively low. This means that there is a lot of empty space in a primitive cell. Figure 5.2 shows the crystalline structure of the same piece that is shown in figure 5.1. From this figure it is easy to see the space that exists in the system. Also, many explain the crystal structure of ice as sheets lying on top of each other.

Without plotting the positron density, it is obvious where it will be strongest. This seems to be a generally large area between these "sheets". So possibly to eliminate those areas, an impurity could be introduced; however, since there is such a large space the molecules could easily flex without being affected as much as copper was.

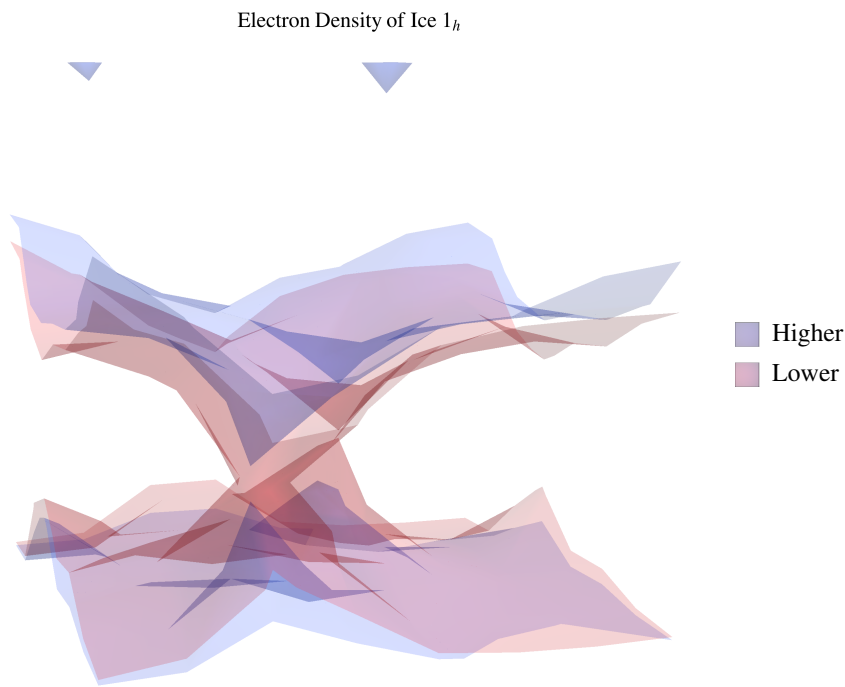


**Figure 5.1** This is an electron density of a pure primitive cell of ice containing 36 atoms.

Oxygen has eight electrons and once hydrogen has interacted with it, the molecule will now have ten electrons. Of these electrons, eight of them are valence electrons. This should show in a very sharp peak when the momentum distribution is calculated, since the majority will have a relatively low momentum (see figure 5.3).

The S and W parameters will be taken from this as a basis, similar to what happened with copper. Once again, the S should be around .5 while the W should be taken at the bottom of the curve. Using this as a comparison for further calculations will be useful.

## 5.2 Ice Vacancy

The hydrogen bond is an electromagnetic attractive interaction between polar molecules. It is not necessarily a true bond, rather it is a particularly strong dipole-dipole at-

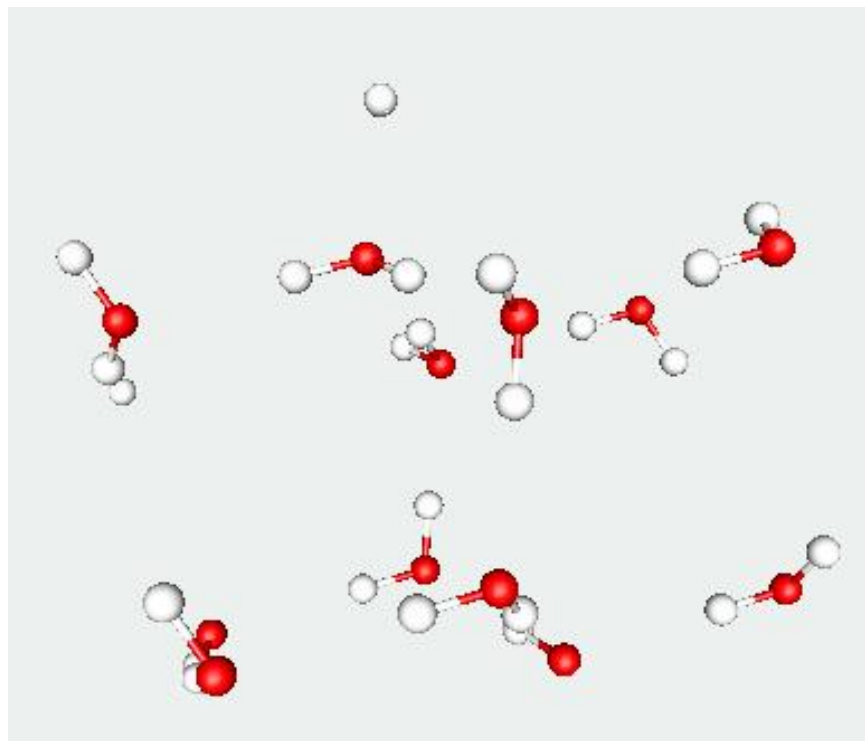


**Figure 5.2** This is a primitive crystalline structure of ice  $1_h$ . It has 36 atoms comprised of 12 oxygen and 24 hydrogen.

traction. It should not be confused with a covalent bond. It is weaker than a covalent or ionic bond, but stronger than a van der Waals interaction [11].

Inside of water there are many lone hydrogen, and oxygen atoms. For this reason there will be three different experiments with vacancies in ice: a hydrogen atom, an oxygen atom, and a  $\text{H}_2\text{O}$  molecule.

Plotting the electron or positron density for each of these three scenarios appears to be close to the same. The sheet of density does change ever so slightly, but nothing that would indicate a grand change from what was observed before.

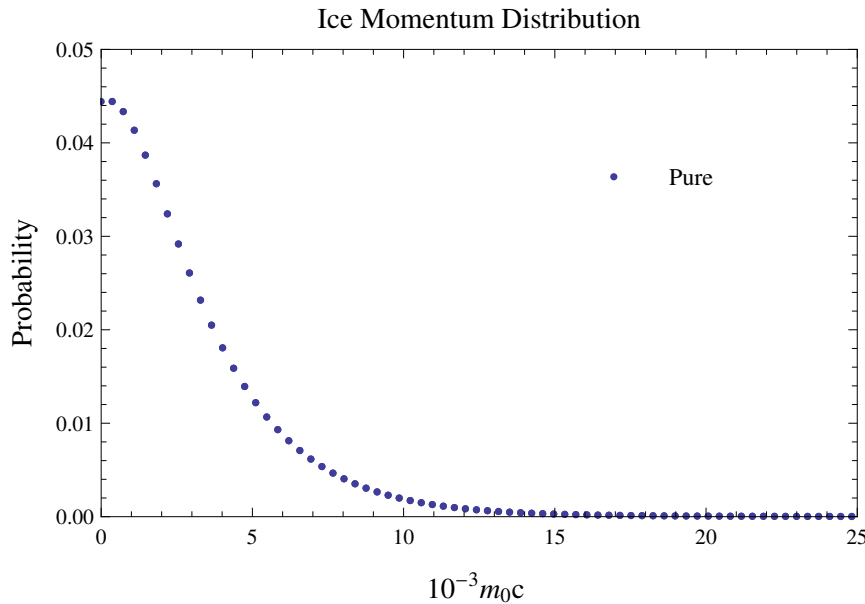


**Figure 5.3** This is a momentum distribution of ice. It has a realitively sharp peak, indicating that the majority of annihilations are occurring with valence electrons.

### 5.3 Ice Analysis

A great comparison of the information gathered is to compare the momentum distribution. In figure 5.4 pure ice, and ice with vacancies of hydrogen, oxygen, and a complete H<sub>2</sub>O molecule are shown. The peak was already sharp with just a pure sample, and as is observed, the peak becomes slightly more sharp, but not much at all.

It appears from looking at the momentum distribution that there might be a detectable difference in the S parameter, but for sure the W parameter will not show a difference. This was slightly predictable from the beginning where it appeared that valence electrons dominated the system.

The S and W parameters for the pure system compared with the different vacancies is shown on the table in figure 5.5. All the parameters are within .008 of the pure sample. This is assurance that it will not be detectable by the detectors that are at

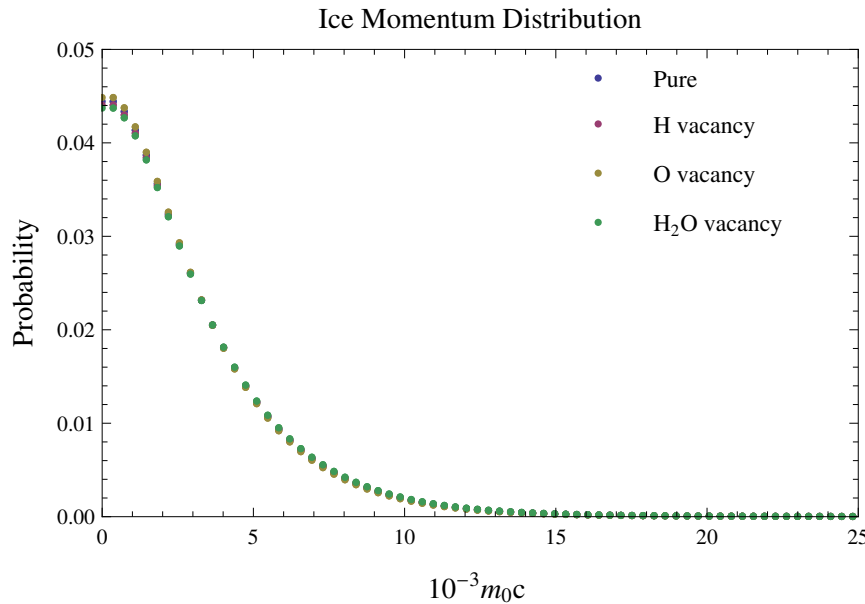


**Figure 5.4** This is a momentum distribution of ice. The four that are plotted are pure, and vacancies of hydrogen, oxygen, and an  $H_2O$  molecule.

Brigham Young University-Idaho.

It is interesting that the  $H_2O$  vacancy had the furthest S parameter from the pure and it was lower. One possible explanation is that there comes the point in the system where taking away molecules increases the percent of core electrons which widens the peak on the momentum distribution. This is still unsure and could be a possible area of future research.

Ice 1 <sub>h</sub> sample	S-parameter	W-parameter
Pure	.516	.153
Hydrogen vacancy	.512	.156
Oxygen vacancy	.520	.151
H <sub>2</sub> O vacancy	.508	.158

**Figure 5.5** The ice sample used in computation is a primitive cell comprised of 36 atoms. These numbers are all in the third significant figure and as such will not be detectable.

# Chapter 6

## Silicon Dioxide

### 6.1 SiO<sub>2</sub> Pure and Vacancy

The last area of interest during this research was silicon dioxide. As seen from figure 3.2, each silicon is interacting with four oxygen atoms. This is completely different from ice 1<sub>h</sub> where each molecule was by itself. The reason silicon was an interest is because of it's mass abundance. This gave an opportunity to not only run computational results, but to also check the results from experiment. Silicon dioxide has however failed to be calculated experimentally. As a result, the conclusions in this section have only computational solidification.

The silicon atom has a tetrahedral coordination with four oxygen atoms surrounding it. The primitive cell has three silicon atoms and six oxygen atoms. Figure 6.1 shows the electron density of the primitive cells. In the center towards the back is a silicon atom with four oxygen atoms attached. One comes out of the page and is attached to another silicon atom.

Plotting the positron density proves to be a little messy and does not reveal as much as the electron density does. Looking at figure 3.2 it is easy to obtain a mental

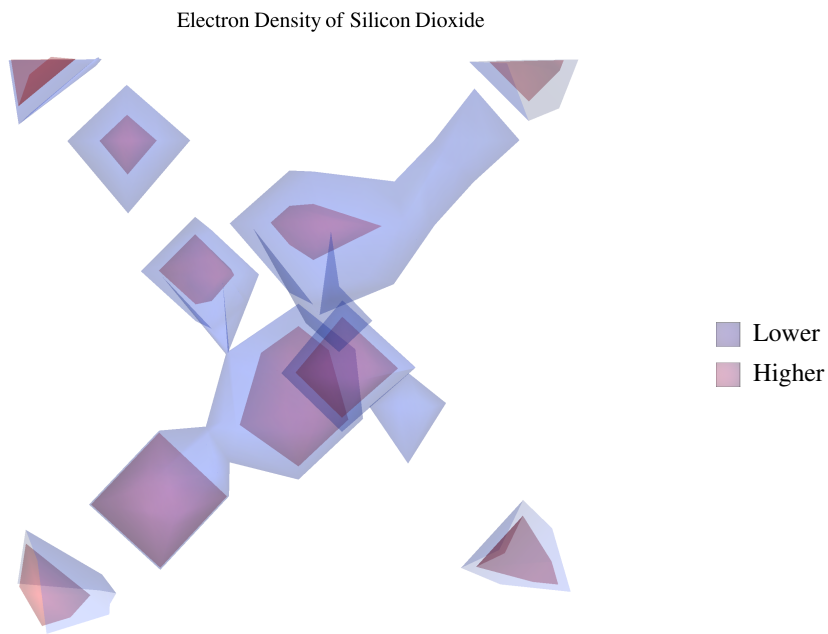


**Figure 6.1** This is the electron density of silicon dioxide. It has nine atoms: three silicon and six oxygens. From the figure, the center towards the back is a silicon with four attached oxygen atoms.

image that the positron densities will be located in the vacancy locations. Since the vacancy spaces are larger, the positron density was not plotted due to the lack of useful information.

Plotting the decomposed momentum distribution of silicon dioxide shows a few interesting things. From figure 6.2, it appears that for any momentum, the most probable annihilation area will be with a valence of an oxygen atom. Also, the higher the momentum goes, the further the valence of oxygen separate themselves from the core electron. This indicates that it will be difficult to notice differences since it appears that even the high momentums have a greater possibility of being produced by a valence electron.

The next stage came in the silicon dioxide research to represent it with a vacancy. Since the silicon would have a greater affect on the system than oxygen, a silicon

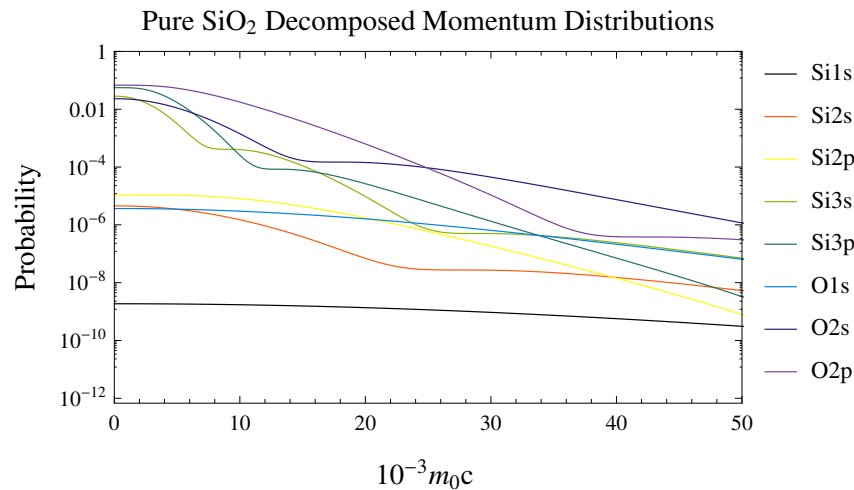


**Figure 6.2** This is the decomposed momentum distribution of silicon dioxide. It shows the shells of both the silicon and oxygen levels. This is comprised of 72 atoms.

atom was removed. From the sample of both copper and ice, introducing a defect in the substance was not detectable. Because of this only a vacancy sample was taken for silicon dioxide.

## 6.2 $\text{SiO}_2$ Analysis

Figure 6.3 shows the normalized comparison of a pure silicon dioxide and a silicon dioxide with a vacant silicon atom. The peak is not as sharp for the silicon dioxide vacancy as it is with the pure. Also the base seems to not taper off as fast as with the pure sample. Just like the practice in copper and ice, the S and W parameters will be taken and compared to each other. The momentum distribution graph makes

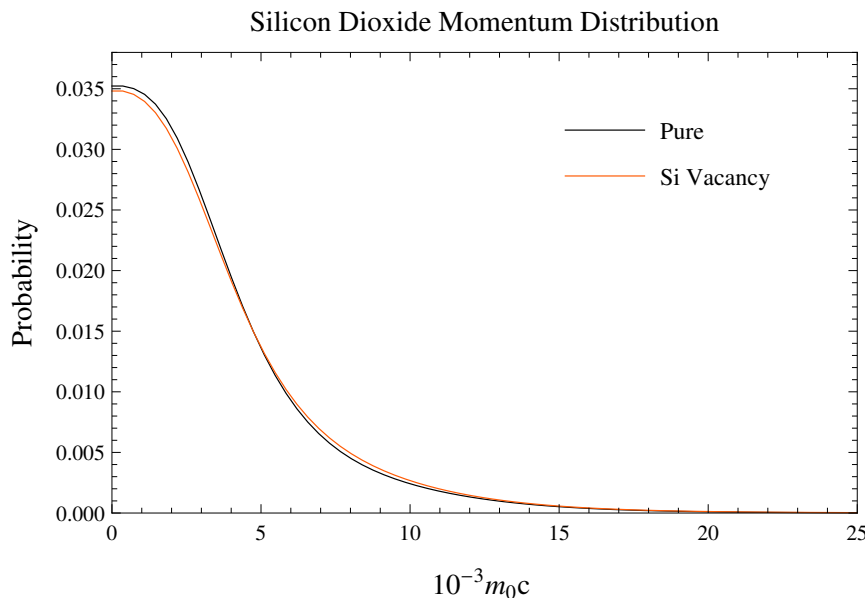


**Figure 6.3** This is the momentum distribution of silicon dioxide. The two lines show a pure silicon dioxide and the other is a silicon dioxide with a missing silicon atom. This is comprised of 72 atoms.

it easier to see where the differences will be observed.

The results obtained were rather interesting. In both the S and W parameter region, the differences are large enough to be measured by a detector. The silicon poor  $\text{SiO}_2$  sample has a smaller S parameter and a larger W parameter (table in figure 6.4).

$\text{SiO}_2$ sample	S-parameter	W-parameter
Pure	.478	.168
Silicon vacancy	.468	.179

**Figure 6.4** The silicon dioxide sample used in computation is a super cell comprised of 72 atoms.

In an effort to understand why the momentum distribution was different than expected, a plot was made comparing the two decomposed momentum distributions. Figure 6.5 shows three different shells from the two samples. The other shells were

observed, but the differences were negligible.

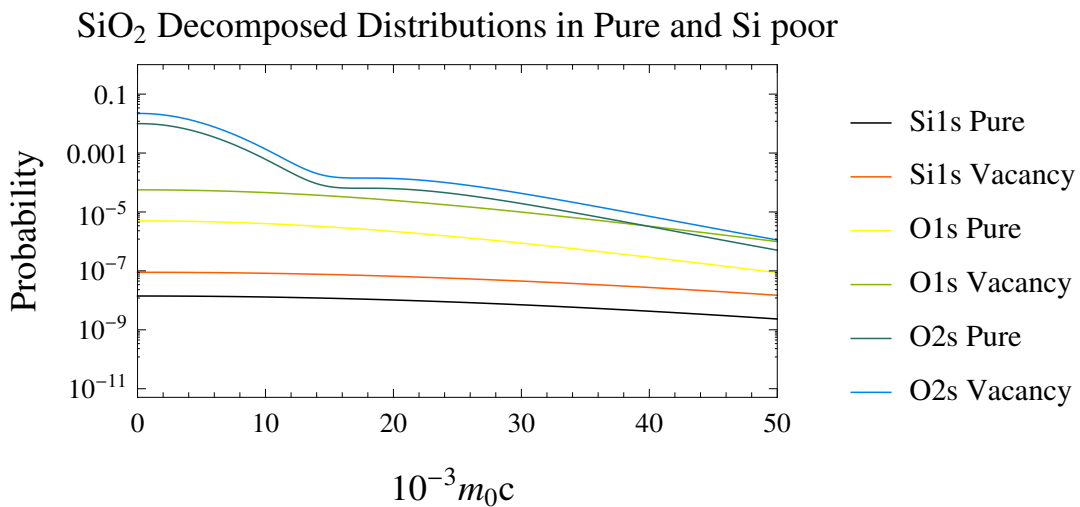


**Figure 6.5** This shows a comparison between three different shells in the two different samples. One is a pure while the other contains one vacant silicon atom. The original has 72 atoms.

The core electrons for both silicon and oxygen increased in probability for the vacancy sample. For the valence electrons, the only noticeable difference was in the first valence shell of oxygen. It was still slightly higher, but the difference was not nearly as much as the two core electron shells. Even though the probability is incredibly small, it makes enough difference to flatten the peak and widen the base on the momentum distribution (figure 6.3). In order for this to make sense the momentum distribution is always normalized.



# Chapter 7

## Conclusion

### 7.1 Analysis

The results obtained by copper was as expected and match reasonably well with experimental data. Knowing that a defect of oxygen will not be noticeable in the outcome will prove useful during future experimental collections.

Ice 1<sub>h</sub> was interesting to model, but does not have many implications on the small level that PAS does. In looking back at figure 1.1, PAS is used in finding extremely small defect sizes. Since ice has such a low packing efficiency and an abundance in valence to core electrons, the defect size will not be detectable.

The results for SiO<sub>2</sub> are slightly different than first expected. Having a missing silicon atom resulted in a flatter peak and wider base. This is opposite of what was observed from copper. The difference was not much, but enough that the detectors should be able to detect it.

## 7.2 Error

Determining the error in a computational program is not a straight forward process. One area where an error could be introduced is in the Density Functional Theory. Rather than solving the many-body wave equation which required the knowledge of the wave already, a different method is required. The Density Functional Theory was used for calculations since the 1970's, but was not considered accurate enough until the 1990's. This is because the theory was refined to better account for the exchange-correlation potential.

Limitations to the theory still exist however. Currently, the theory is not able to describe intermolecular interactions such as the van der Waals forces (forces between dipoles), transition states, dopant interactions, and calculations of ferromagnetism in semiconductors [12]. There exists a current and ongoing development to enhance the Density Functional Theory by accounting for both core and valence electrons and other molecular interactions.

The research conducted in this thesis is not affected by these limitations of the DFT that have been described. An approved method is to compare the computational results with approved experimental results, or results taken in a lab. A strong correlation would suggest that the theory is correct and accurate for our purposes. This correlation does exist and helps confirm that the computational work is accurate to the level desired.

Another possible area of error is in the multigrid method. One way to track this error is to monitor the calculated total energy as the system is moved with respect to the grid. A numerical grid will break translational symmetry. This implies that the calculation is dependent on where the molecule is positioned relative to the grid. To solve or limit this issue a correct prolongation operator is used in the electron density

to return to the coarse grid equation 2.16.

Calculation time rises rapidly with increasing the number of grid points while not enough will give bad results. To help find the balance between the two, start with a low number of grid point and continue working up while results are still changing. Supercells that have more than 200 atoms required around  $80^3$  grid points.

### 7.3 Future Research

There are many different areas that could be explored from this point. One that is particularly interesting is heterogenous mixtures, meaning for example having a unit cell of ice imbedded into a copper supercell. A supercell is a composition of many unit cells. Along with this research it would be useful to see how plausible that is.

In the copper section there was a S and W parameter for data that was done experimentally. The copper was brushed over with sand paper. This introduced impurities into the system, or perhaps created vacancies. Copper with many different impurities and defects needs to be modeled computationally to help understand the experimental data.

For a vacuum chamber one of the challenges comes outgassing. This is where molecules or even single atoms come out from inside the chamber wall. While at room pressure, atoms are forced into the chamber walls and when the chamber is brought down to pressure the atoms come out from the walls. This is detected as a leak and can produce problems in getting to low pressures. It would be interesting to model the metal that is upstairs in the vacuum chamber for the physics department and take a sample to analyze. The sample can be exposed to positron annihilation to take experimental data. Then the computational part begins to model what was taken as results.

A large part of this research was done representing silicon dioxide. However, we were never able to take a sample and expose it to positron annihilation to compare the results. The geology department has a large supply of silicon dioxide and I have confidence that if the right person was to ask the department chair, the department would let us borrow a sample to analyze.

The silicon dioxide was interesting in that introducing a silicon vacancy showed the opposite of what was expected. Making other calculations are necessary, such as introducing an oxygen vacancy, and possibly an entire  $\text{SiO}_2$  molecule. After this was done, examining the difference in the decomposition would help to understand from where the shift is coming. Also, doing a little more research to know what impurities are common in  $\text{SiO}_2$ , then doing the computational analysis would be interesting to do.

Performing the convolution on computational data was not a trivial process. For this thesis I was able to show the results of a convolution from a gaussian at FWHM from the original data. The convoluted surface matched closely with experimental data but seemed to be shifted slightly. To compare with the results taken off the detectors at BYU-Idaho, a knowledge is needed of how much the detectors affect the data. Once this information is obtained, the convolution will be able to represent the affect of the detectors and should mimic the experimental data.

# Bibliography

- [1] Hartley, J.H., Howell, R.H., Asoka-Kumar, P, Sterne, P.A., Akers, D., Denison, A., "Positron annihilation studies of fatigue in 304 stainless steel", *Appl. Surf. Sci.*, 149, 199, 204
- [2] Torsti, T., Lindberg, V., Makkonen, I., Ogando, E., Rasanen, E., Saarikoski, H., Puska, M. J., and Nieminen, R. M., "MIKA - a multigrid-based program package for electronic structure calculations" *Laboratory of Physics, Helsinki University of Technology* 2005
- [3] Gagliardi, Marcus A., "Positron Defect Mapping" *Idaho State University*, September 2008
- [4] Rice-Evans, P.C., Saleh, A.S., Bull, S.J., "Positron beam spectroscopy for the assessment of the structure and defect density of titanium nitride" *Physics Department, University of London* May 1994
- [5] Kantorovich, Lev, "Quantum Theory of the Solid State: An Introduction", *Springer* 2004
- [6] Chaplin, Martin, "Water Structure and Science", 2014  
<http://www1.lsbu.ac.uk/water/phase.html>

- [7] Burns, Gerald, Glazer, A.M., "Space Groups for Solid State Scientists" Second Edition *Harcourt Brace Jovanovich, Publishers* 1990
- [8] American Mineralogist Crystal Structure Database  
<http://rruff.geo.arizona.edu/AMS/amcsd.php>
- [9] Nelson, Lance, "Cluster Expansion Models Via Bayesian Compressive Sensing", *Brigham Young University*, May 2013
- [10] Brandt, A., "Multi-level adaptive solutions to boundary-value problems" *Math. Comput.*, 31, 1993
- [11] International Union of Pure and Applied Chemistry, "Compendium of Chemical Terminology", 2nd ed. (the "Gold Book") (1997)
- [12] Assadi, M.H.N "Theoretical Study on copper's energetics and magnetism in TiO<sub>2</sub> polymorphs" *Journal of Applied Physics* 113 2013

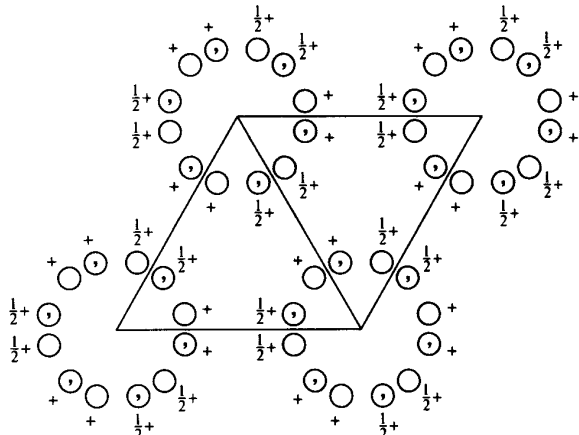
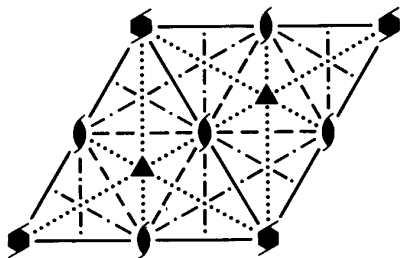
# Appendix A

## Crystallography

$P6_3cm$  $C_{6v}^3$  $6mm$ 

Hexagonal

No. 185

 $P6_3cm$ Patterson symmetry  $P6/mmm$ Origin on  $31m$  on  $6_3cm$ 

<b>Asymmetric unit</b>	$0 \leq x \leq \frac{2}{3}; \quad 0 \leq y \leq \frac{1}{2}; \quad 0 \leq z \leq \frac{1}{2}; \quad x \leq (1+y)/2; \quad y \leq \min(1-x, x)$
Vertices	$(0, 0, 0) \quad \frac{1}{2}, 0, 0 \quad \frac{2}{3}, \frac{1}{3}, 0 \quad \frac{1}{3}, \frac{2}{3}, 0$ $(0, 0, \frac{1}{2}) \quad \frac{1}{2}, 0, \frac{1}{2} \quad \frac{2}{3}, \frac{1}{3}, \frac{1}{2} \quad \frac{1}{3}, \frac{2}{3}, \frac{1}{2}$

**Symmetry operations**

- |                                    |                                      |                                      |
|------------------------------------|--------------------------------------|--------------------------------------|
| (1) 1                              | (2) $3^+ 0, 0, z$                    | (3) $3^- 0, 0, z$                    |
| (4) $2(0, 0, \frac{1}{2}) 0, 0, z$ | (5) $6^-(0, 0, \frac{1}{2}) 0, 0, z$ | (6) $6^+(0, 0, \frac{1}{2}) 0, 0, z$ |
| (7) $c x, \bar{x}, z$              | (8) $c x, 2x, z$                     | (9) $c 2x, x, z$                     |
| (10) $m x, x, z$                   | (11) $m x, 0, z$                     | (12) $m 0, y, z$                     |

**Generators selected** (1);  $t(1,0,0)$ ;  $t(0,1,0)$ ;  $t(0,0,1)$ ; (2); (4); (7)

### Positions

Multiplicity,  
Wyckoff letter,  
Site symmetry

### Coordinates

### Reflection conditions

General:

12 $d$ 1	(1) $x, y, z$	(2) $\bar{x}, x-y, z$	(3) $\bar{x}+y, \bar{x}, z$	$h\bar{h}0l : l = 2n$			
	(4) $\bar{x}, \bar{y}, z + \frac{1}{2}$	(5) $y, \bar{x}+y, z + \frac{1}{2}$	(6) $x-y, x, z + \frac{1}{2}$	$000l : l = 2n$			
	(7) $\bar{y}, \bar{x}, z + \frac{1}{2}$	(8) $\bar{x}+y, y, z + \frac{1}{2}$	(9) $x, x-y, z + \frac{1}{2}$				
	(10) $y, x, z$	(11) $x-y, \bar{y}, z$	(12) $\bar{x}, \bar{x}+y, z$				
6 $c$ . . $m$	$x, 0, z$	$0, x, z$	$\bar{x}, \bar{x}, z$	$\bar{x}, 0, z + \frac{1}{2}$	$0, \bar{x}, z + \frac{1}{2}$	$x, x, z + \frac{1}{2}$	Special: as above, plus no extra conditions
4 $b$ 3 . .	$\frac{1}{3}, \frac{2}{3}, z$	$\frac{2}{3}, \frac{1}{3}, z + \frac{1}{2}$	$\frac{1}{3}, \frac{2}{3}, z + \frac{1}{2}$	$\frac{2}{3}, \frac{1}{3}, z$			$hkil : l = 2n$
2 $a$ 3 . $m$	$0, 0, z$	$0, 0, z + \frac{1}{2}$					$hkil : l = 2n$

### Symmetry of special projections

Along [001]  $p6mm$   
 $\mathbf{a}' = \mathbf{a}$      $\mathbf{b}' = \mathbf{b}$   
Origin at  $0, 0, z$

Along [100]  $p1m1$   
 $\mathbf{a}' = \frac{1}{2}(\mathbf{a} + 2\mathbf{b})$      $\mathbf{b}' = \frac{1}{2}\mathbf{c}$   
Origin at  $x, 0, 0$

Along [210]  $p1g1$   
 $\mathbf{a}' = \frac{1}{2}\mathbf{b}$      $\mathbf{b}' = \mathbf{c}$   
Origin at  $x, \frac{1}{2}x, 0$

### Maximal non-isomorphic subgroups

I	[2] $P6_311$ ( $P6_3$ , 173)	1; 2; 3; 4; 5; 6
	[2] $P3c1$ (158)	1; 2; 3; 7; 8; 9
	[2] $P31m$ (157)	1; 2; 3; 10; 11; 12
	{ [3] $P2_1cm$ ( $Cmc2_1$ , 36) }	1; 4; 7; 10
	{ [3] $P2_1cm$ ( $Cmc2_1$ , 36) }	1; 4; 8; 11
	{ [3] $P2_1cm$ ( $Cmc2_1$ , 36) }	1; 4; 9; 12

IIa    none

IIb    [3]  $H6_3cm$  ( $\mathbf{a}' = 3\mathbf{a}$ ,  $\mathbf{b}' = 3\mathbf{b}$ ) ( $P6_3mc$ , 186)

### Maximal isomorphic subgroups of lowest index

IIc    [3]  $P6_3cm$  ( $\mathbf{c}' = 3\mathbf{c}$ ) (185); [4]  $P6_3cm$  ( $\mathbf{a}' = 2\mathbf{a}$ ,  $\mathbf{b}' = 2\mathbf{b}$ ) (185)

### Minimal non-isomorphic supergroups

I	[2] $P6_3/mcm$ (193)
II	[3] $H6_3cm$ ( $P6_3mc$ , 186); [2] $P6mm$ ( $\mathbf{c}' = \frac{1}{2}\mathbf{c}$ ) (183)



## Appendix B

### INPUT H2O\_36

```
2 0 .FALSE. .TRUE. .FALSE.          # 1
.FALSE. .FALSE.
0.22 0 1 0.01
.FALSE.
12 24                      # 2
0 H                         # 3
3 1                         # 4
14.77766 0.5 1.0           # 5
32 32 32 12. 1d-12         # 6
9999999999.9 1.0 1.    was: 9999999999.
1. 0. 0.                      # 7
0. 1. 0.                      # 8
0. 0. 0.94117                # 9
1 1 0.3333 0.0 0.0625 0.0    # 10
1 2 0.83335 0.288646267 0.0625 0.0
1 3 0.3333 0.577292534 0.0625 0.0
1 4 0.6666 0.0 0.5625 0.0
1 5 0.6667 0.577292534 0.5625 0.0
1 6 0.16665 0.288646267 0.5625 0.0
1 7 0.6666 0.0 0.9375 0.0
1 8 0.6667 0.577292534 0.9375 0.0
1 9 0.16665 0.288646267 0.9375 0.0
1 10 0.3333 0.0 0.4375 0.0
1 11 0.83335 0.288646267 0.4375 0.0
1 12 0.3333 0.577292534 0.4375 0.0
2 1 0.3333 0.0 0.174 0.0
2 2 0.83335 0.288646267 0.174 0.0
2 3 0.3333 0.577292534 0.174 0.0
2 4 0.6666 0 0.674 0.0
2 5 0.6667 0.577292534 0.674 0.0
```

```
2 6 0.16665 0.288646267 0.674 0.0
2 7 0.438 0 0.026 0.0
2 8 0.781 0.379319127 0.026 0.0
2 9 0.281 0.486706277 0.026 0.0
2 10 0.562 0 0.526 0.0
2 11 0.719 0.486706277 0.526 0.0
2 12 0.219 0.379319127 0.526 0.0
2 13 0.7195 0.0909326674 0.975 0.0
2 14 0.5615 0.577638944 0.975 0.0
2 15 0.219 0.197453792 0.975 0.0
2 16 0.7805 0.775092736 0.475 0.0
2 17 0.9385 0.288386459 0.475 0.0
2 18 0.281 0.668571612 0.475 0.0
2 19 0.781 0.197453792 0.475 0.0
2 20 0.2805 0.0909326674 0.475 0.0
2 21 0.4385 0.577638944 0.475 0.0
2 22 0.719 0.668571612 0.975 0.0
2 23 0.2195 0.775092736 0.975 0.0
2 24 0.0615 0.288386459 0.975 0.0
1.0 5000
```

The pound symbol followed by an integer leading from one to ten is not part of the INPUT. They were place there and given a reference to this page where I will discuss each one a little more. If I did not include a hash tag, then the line was left default.

1. The first integer in this row indicates the number of atom types. So the number of different elements that the INPUT file will be representing.
2. This row correlates with the atom types. For example if two atom types are selected, then there needs to be two integers in this row. The integer specifies the amount of atoms in each atom type. The order needs to be in the same order as the following row. In other words there are going to be 12 Oxygen and 24 Hydrogen.
3. The element symbol of the atoms being used. For this INPUT it is Oxygen and Hydrogen. Hydrogen is not in the original MIKA folder and needed to be added in the MIKA/doppler/MIKADoppler\_user/FREE\_AT\_IN/atominput/<file>. It will need to be in a certain format, so a close observation at the other atom inputs in the folder will help.
4. Once again this row needs to correlate with the rows above. The first being attached to Oxygen and the second to copper. The integer indicates the number of electron shells that the user wants.
5. The first floating number in this row specifies the lattice constant in atomic units. This should be from a reppitable source and is the length of one side of the lattice. For ice, the x and y are the same length, but the z is slightly shorter. This can be adjusted on #7-#9.

6. The first three integers are the number of grid points in the x,y,z directions. The manual suggests using values that are dividable by  $2^n$ . The more grid points will lead to a slower calculation. However, if a system has more than 200 particles at least 80 grid points in each direction are needed.
7. The x lattice vector. These are to be given in cartesian coordinates. If a supercell is being modeled, here is where you would make the change.
8. The y lattice vector.
9. The z lattice vector. To obtain this value, find the proportion of the lattice length that is in the z direction and that is what goes here.
10. From here on it is a list of all the atoms. The first integer is defining which element it is. The second integer is a count of the atoms of that specific element. The next three floats are the position of that atom. After each x,y,z positions there is a 0.0 This is by default and that is how I kept it. It tells the MIKA program that the information for that specific atom is now finished, so return to the next line and continue.

# Index

- Agglomeration, 18
  - prolongation, 19, 54
  - restriction, 18
- Annihilation, 3–6
  - rate, 20
- Converge, 18, 19
- Convolution, 29, 38, 56
- Cross section, 20
- Dextrorotatory, 8
- Energy
  - $\gamma$  rays, 3
  - annihilation, 5
  - conservation, 4
  - exchange-correlation, 12, 14, 20
  - ground-state, 12, 16
  - total, 15, 54
- Enhancement factor, 21
- Gamma ray, 3–5
- Gaussian, 5, 15
  - FWHM, 29, 35, 56
- Grid point, 28, 55, 66
- Interaction
  - annihilate, 3
  - dopant, 54
  - electromagnetic, 42
  - electron-electron, 12
  - electron-nuclei, 11
  - ion-ion, 16
  - molecular, 54
  - van der Waals, 43, 54
- Kohn-Sham
- equation, 11, 16
  - potential, 11
  - theorem, 12–13
- Laevorotatory, 8
- Lifetime, 2, 5, 21, 23
- Local density approximation, 14, 20
- Method
  - Gauss-Seidel, 19
  - Jacobi, 17, 19
  - Rayleigh quotient, 19, 36
- Packing efficiency, 7, 41, 53
- Point group, 7
- Potential
  - coulomb, 12
  - exchange-correlation, 11–14, 19, 54
  - external, 11
  - Hartree, 11, 14–15, 19
  - Kohn-Sham, 11
  - pseudo, 15
- Schrödinger equation, 11–12
- Shot peening, 2
- Space group, 2, 6, 58
  - cubic, 7
  - ice  $1_h$ , 7
  - $\text{SiO}_2$ , 8
- Wave
  - equation, 11, 54
  - function, 5, 6, 20
  - pseudo, 15
- Wyckoff position, 7, 9